Geomorphology 446 (2024) 108979

Contents lists available at ScienceDirect

Geomorphology

journal homepage: www.journals.elsevier.com/geomorphology

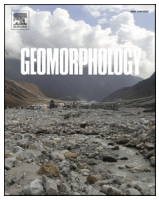

Mass movement hazard & global climate change: Physical-deterministic modelling study of the rest and be thankful pass, Scotland UK

Niels R. Klaver [a], Tom A. Dijkstra [b], Andrew Barkwith [c], Claire Dashwood [c], Steven M. De Jong [a,*], Rens L.P.H. van Beek [a]

[a] Department of Physical Geography, Utrecht University, Netherlands
[b] School of Architecture, Building and Civil Engineering, Loughborough University, UK
[c] British Geological Survey, Keyworth, UK

ARTICLE INFO

Keywords:
Mass movement trigger
Road closure
Precipitation scenarios
CLiDE-Model

ABSTRACT

Mass movements frequently affect infrastructure corridors, particularly so in mountainous areas. The A83 at the Rest and be Thankful pass (Scotland, UK) is a prime example of a road experiencing frequent closure due to precipitation-triggered landslides and debris flows. The closures result in long (>90 km) diversions and severe economic losses (>£60 million). To ensure persistence of transport services, future engineered interventions and maintenance schedules must anticipate the potential consequences of climate change that affects the frequency and magnitude threshold precipitation events that are capable of triggering mass movement. In turn this requires a better understanding of the hydrological implications of climate change on precipitation-triggered landslides and debris flows. The area is prone to mass movements due to steep topography, the glacial history, reworked deposits of mud and siltstone, and landslide-triggering precipitation. The objective here is to assess the severity of future events, i.e. the coming decades, was assessed by means of an event-based runout model for selected events that were identified using a present-day precipitation threshold applied to hydro-meteorological forecasts for this part of the UK. A convex hull method was applied to these forecasts to create a comprehensive selection of modelled events and a much reduced computational load. This selection is considered to be representative for the largest variation within the forecasts.

Results show that 61 mm of daily precipitation will likely trigger mass movement. This threshold reduces by 0.15 mm for every millimetre accounted for in an antecedent precipitation index calculated based on 8 antecedent days. On the basis of the hydro-meteorological forecasts it can be concluded that the frequency of these trigger conditions gradually declines, as seven out of the eleven RCM (Regional Climate Model) configurations show longer recurrence intervals. This corresponds with the decline in the modelled future precipitation. However, it is observed that, for scenarios with lower average daily precipitation and antecedent precipitation indices, event severity is likely to increase as intense daily precipitation follows drier antecedent conditions. For scenarios with higher average daily precipitation and antecedent precipitation indices, persistent wetting appears to expand source areas and increases material entrainment. The simulations show that the main source areas, situated between 300 and 500 metre elevation, extend upslope when the antecedent precipitation regime has peak precipitation values in the latter stages of the 8 antecedent days.

1. Introduction

Mass movements pose a major threat to infrastructure corridors and this can be particularly severe in mountainous areas (Kromer et al., 2015; Jaiswal and van Westen, 2009; Schlögl and Matulla, 2018; Hearn and Massey, 2009). The consequences of landslides disrupting transport routes can be significant; it can lead to fatalities, damage to livelihoods and isolation of communities. The A83 at the Rest and be Thankful (RaBT) pass in Northern Scotland is a sad but relevant example of an important national road frequently closed due to mass wasting. This especially impacts the access of the cut off area to emergency services due to >90 km detours. The identification of hazards along transport routes has therefore attracted much interest (Kjekstad and Highland, 2009; Hearn, 2011; Bee et al., 2019).

* Corresponding author.
E-mail address: s.m.dejong@uu.nl (S.M. De Jong).

https://doi.org/10.1016/j.geomorph.2023.108979
Received 22 March 2023; Received in revised form 9 November 2023; Accepted 13 November 2023
Available online 22 November 2023

There is increasing recognition that our changing climate needs to be considered as part of the hazard and risk assessment of transport networks (Postance et al., 2017; Winter et al., 2008, 2018; Winter and Corby, 2012). The hydrological triggering of mass movement (Van Asch et al., 1999; Iverson, 2000) is part of complex, dynamic system affected by climate change and this should be accounted for in hazard assessment of transport networks. However, this is complicated due to the complex response of climate systems to changing atmospheric greenhouse gas concentrations, uncertainties in estimating the resulting hydro-meteorological trends, and difficulties in the parameterisation and process description of hydro-meteorologically triggered mass movements.

Scotland's trunk road network carries some 35 % of all traffic and has a total asset value exceeding £23 billion (Transport Scotland, 2018). Several key corridors in this network are frequently affected by mass movement (Winter et al., 2016), with subsequent disruption of services having a major impact on local communities and the Scottish economy (Winter et al., 2008; Wong and Winter, 2018). One of these vulnerable corridors is the A83 which connects Glasgow to Inverary and the council area Argyll & Bute with over 4000 vehicles passing daily (Finlayson, 2020). Particularly at the Rest and Be Thankful pass (RaBT), debris flows have resulted in disruptive road closures (Fig. 1; Table 1; Postance et al., 2017; Winter, 2014; Winter and Shearer, 2017; Bee et al., 2019; McMillan and Holt, 2019; Finlayson, 2020). Consequently, the Scottish Government invested in major engineered interventions in the form of ring net systems to capture debris flow events, the re-establishment of a diversion route positioned along the lower slopes to carry traffic in case the main A83 would be blocked and plans to change local land use to reduce the risk of slope instability (Macklin, 2013; Winter and Corby, 2012; Winter, 2020).

The dominant mass movement type affecting the RaBT slopes involves relatively shallow, translational slides (Fig. 2) of colluvium material that are triggered by intensive precipitation and precipitation in the preceding days. These slides rapidly transform into debris flows, capable of entraining gully-based deposits (e.g. Winter et al., 2010). The objective of our study is to improve our understanding of the implications of climate change on the manifestation of mass movements on the RaBT slopes. Climate projections for the next decades are used to assess future hydrological conditions. A modelling platform is used to account for these future hydrological conditions, to use terrain and soil information, to assess the frequency of future triggering events for mass movements and to visualize the impact on local slope stability above the national A83 road. Information about the study site will be given in the next section followed by the methodology and datasets.

Table 1
Dates of the recorded historical mass movement events along the highway A83 and causing traffic disruptions. The table presents days of closure and the associated estimated displaced mass obtained from BGS (2018) and the analysis of news articles. Details are available in the British Geological Survey Geoindex: www.bgs.ac.uk/map-viewers/geoindex/.

Date	Displaced mass (kg)	Closure days
11 12 2020	–	1
09 13 2020	1,000,000	10
08 2 2020	30,000,000	35
01 30 2020	1,300,000	1
10 9 2018	3,000,000	9
12 30 2015	250,000	6
12 5 2015	1,000,000	0
10 28 2014	2,000,000	1
10 1 2013	100,000	1
08 1 2012	1,000,000	2
02 1 2012	40,000	2
09 8 2009	730,000	2
10 28 2007	400,000	14

2. Study site

The study area is located in western Scotland approximately 60 km northwest of Glasgow shown in Fig. 1. Emphasis is put on the most unstable slopes southeast of the viewpoint at the top of the pass and indicated by the red lines in Fig. 1. The geologic formation under the local steep slopes consists mainly of schists of metamorphic origin. These rocks are commonly intensely foliated and folded. More important for the mass movements than the underlying rocks are the slope

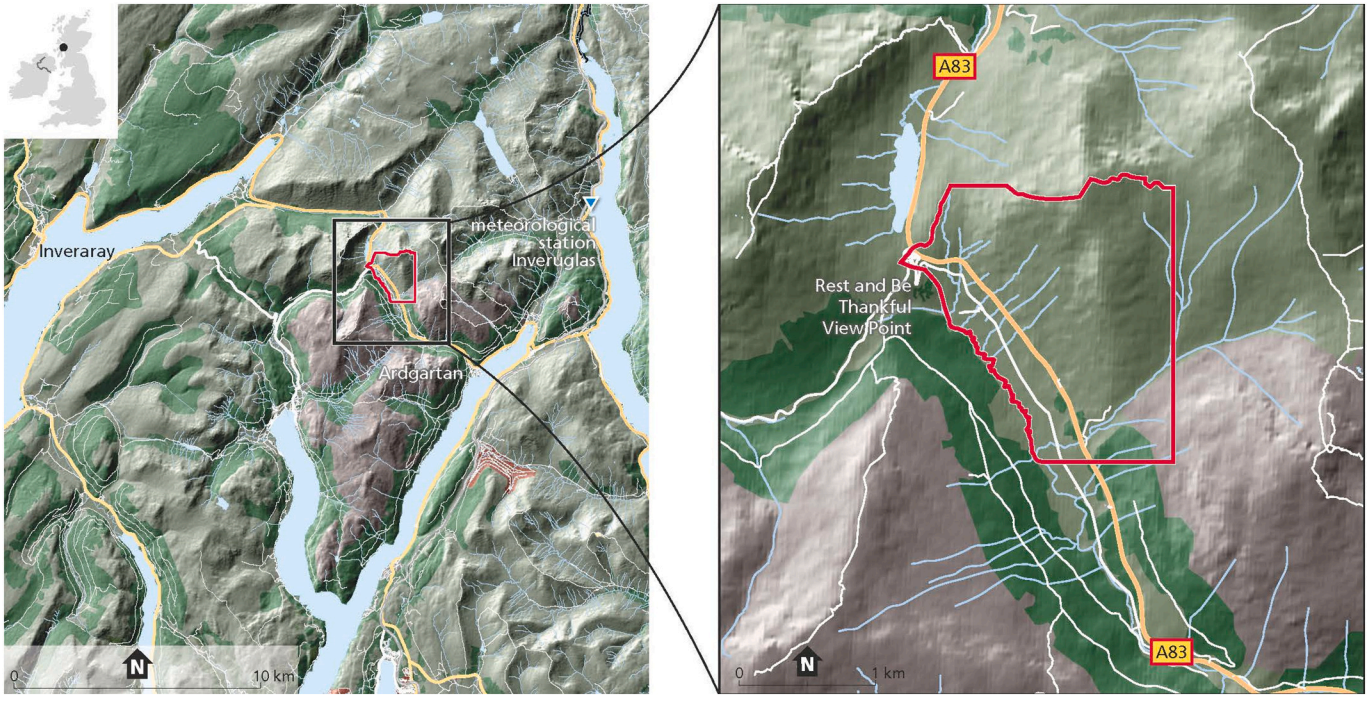

Fig. 1. Location and overview of the Rest and Be Thankful pass in North-Western Scotland. The red outline indicates the model area of this study. The blue markers denote the weather stations from which the rainfall time series have been obtained.

Fig. 2. Field picture showing the steep topography, the shallow landslides and the debris flows and their incisions above and the A83 at the Rest and Be Thankful pass. Note the cars and bus for scale. The upper road is the road for the public and the lower road is a military road.
Source: David Petley on AGU blog (blogs.agu.org/landslideblog/2020/10/09/rest-and-be-thankful/).

deposits. This colluvium comprise sandy to gravelly silts and clays with varying amounts of boulders and material of earlier mass wasting. The geomorphology of the RaBT pass is largely governed by the glaciation of the late Devensian (Tanner et al., 2013). Finlayson (2020) delivers the most detailed geomorphological assessment of this region to date. Glacial retreat occurred between 12.9 and 11.5 kyr BCE and paraglacial lacustrine and fluvial deposition took place on the flanks of southern Beinn Bheula mountain during this period located just south of the pass. Subsequent erosion has resulted in the extensive reworking and redistribution of the slope material and therefore it is difficult to trace the original glacial and para-glacial drift (Ballantyne, 2002, 2004; Finlayson, 2020). As a result, the present geomorphology is characterised by extensive gully systems, incising mixed and poorly sorted paraglacial deposits, that overlay the Schist Formation. Evidently, giving the geomorphological nature of the study site, the hillslope deposits are very thin. The shallow translational slides and debris flows observed at the RaBT-pass are largely initiated by excessive pore pressures resulting from intense precipitation events (Iverson, 2000; Sparkes et al., 2017). These precipitation events are common in the wet climate of Western Scotland, which is characterised by an annual average precipitation of 3180 mm (Scottish Environmental Protection Agency, 2017); an annual maximum temperature of 11.3; and an annual minimum temperature of 4.8 (MetOffice, 2019).

The RaBT slope (Figs. 1 and 2) largely remains in a condition of marginal stability, as evidenced by frequent mass movements closing the A83 eleven times between 2007 and 2017 (totalling nearly 30 days; Table 1). These closures have had a major impact. Winter et al. (2018) describes a vulnerability shadow of these events stretching from just north of Glasgow along the A83 to the town of Oban. Postance et al. (2017) illustrate the regional impact through a traffic modelling exercise. Fortunately, mass movement events at this site have not resulted in fatalities, but transport diversions up to 96 km have led to substantial economic costs (with estimated daily costs ranging between £52 thousand (Macklin, 2013) and £80 thousand (Postance et al., 2017)). From 2007 until 2016 more than £63 million GBP was invested in measures to mitigate the effects of mass movements at the RaBT-pass, including catch pits, boulder stabilisers, netting, barriers and the re-establishment of the Old Military Road as a diversionary route. Transport Scotland went through a public consultation process to identify alternative route corridors, but this corridor across the RabT-pass remains the quickest and most cost-effective to deliver (Transport Scotland, 2021). Measures continue to be implemented to reduce the impact of mass movements on the transport system. However, to better inform operation and maintenance investment strategies at this site, it is important to evaluate future changes in slope stability.

3. Materials & methods

The modelling approach in this study strives to assess the hazards for mass movements above this road for the coming decades. This research uses the United Kingdom Climate Projections (UKCP09) forecasts (Murphy et al., 2009; Chan et al., 2018) to model and evaluate how and to what extent a changing climate may affect the frequency of mass movements disrupting the A83 up to year 2050. It is intended to identify conditions for the triggering of mass movement at RaBT-pass that are based on thresholds of coupled antecedent precipitation and daily rainfall. Fig. 3 presents a flow diagram of the approach. This modelling approach enables the quantitative coupling of model simulations of future meteo-hydrological conditions with a model simulating mass movements and accounting for triggering rainfall events and antecedent moisture conditions. The outcome provides insight in future landslide hazards on the mountain pass.

The training period is based on a decade of observations from 2007 until 2017, the historic data in Fig. 3. These thresholds are then

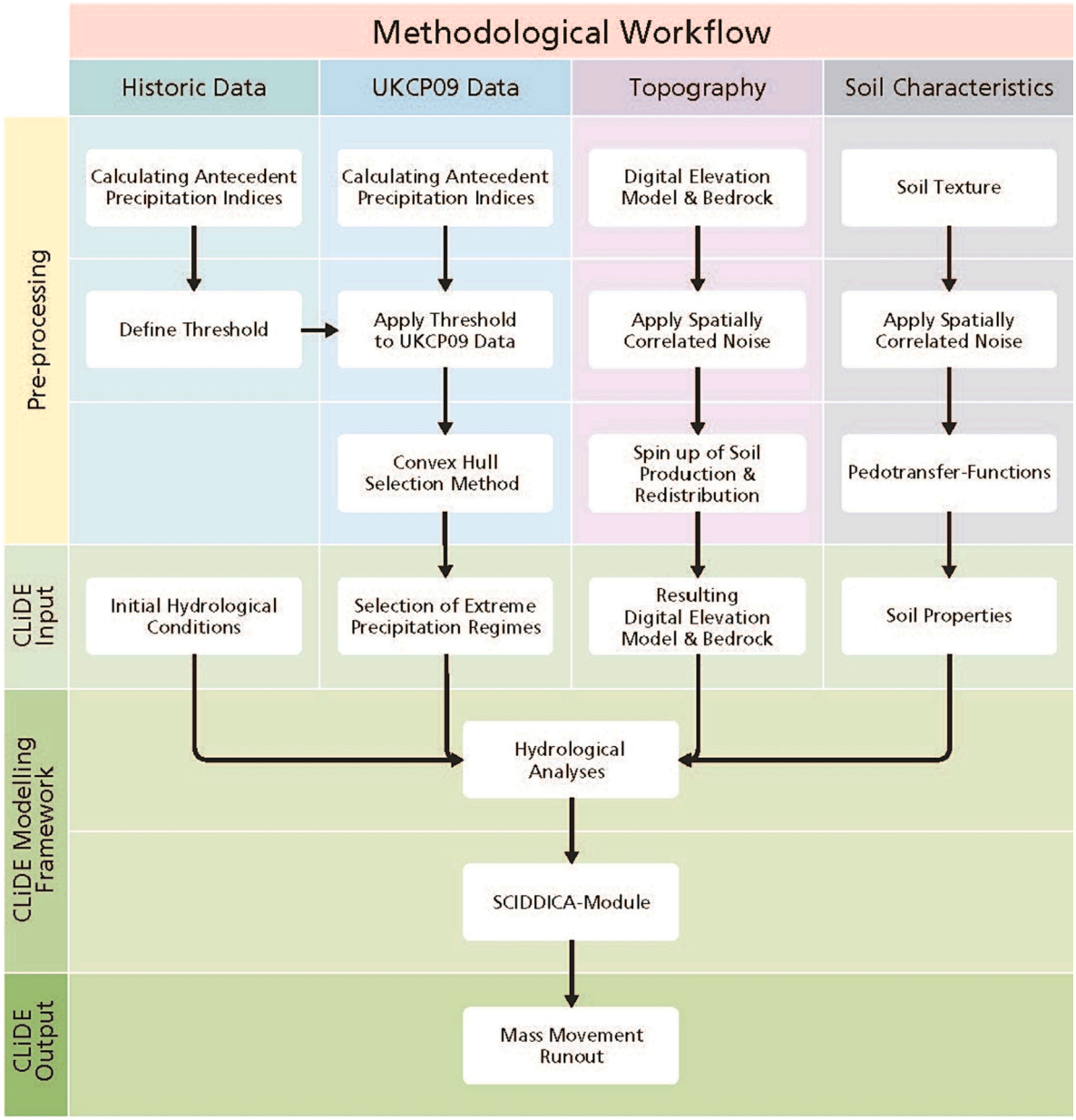

Fig. 3. Methodological workflow as applied in this study for modelling. The upper part shows the preparation phase for model input where antecedent and daily precipitation is related to triggering of mass wasting providing thresholds for the scenarios, climate projections for the coming decades are collected and topographic and soil data are prepared. The CLiDE modelling platform (Barkwith and Coulthard, 2014) is used to quantitatively simulate future hydrological conditions. The SCIDDICA-module within CLiDE simulates the mass movements based on evolving hydrological conditions. Running scenarios allow the assessment of future slop instability.

evaluated in the context of the UKCP09 forecasts (Murphy et al., 2007; Christierson et al., 2012) to identify future critical rainfall episodes and assess changes in frequency of occurrence. Detailed simulations are performed on a selection of these critical rainfall episodes. This selection is representative for the largest possible variation in rainfall and antecedent precipitation regimes that can trigger mass movement at the study site. It is therefore based on sampling of the convex hull (Andrew, 1979) of all threshold exceeding events. The hydrological response to these selected episodes and subsequent initiation and propagation of mass movement along the slope of the RaBT-pass is simulated to delineate the extent of mass movements that may interrupt traffic.

3.1. Precipitation thresholds

To evaluate the hydro-meteorological conditions that lead to slope failure, we analysed daily precipitation and antecedent precipitation indices or APIs (Bruce and Clark, 1966; Glade et al., 2000) corresponding to historical mass movement events shown in Table 1. Plotting daily precipitation versus APIs for 4, 8 and 12 antecedent days of precipitation enables deduction of a hydro-meteorological threshold envelope. The choice of 4, 8 and 12 days is based on earlier work of Glade et al., 2000 indicating that an appropriate length of antecedent days is around 10 days. The input is a continuous precipitation dataset covering the period from 2007 to 2017 (Scottish Environmental Protection Agency, 2017), based on fifteen-minute interval measurements that are aggregated to daily values. Rain gauges were installed in late April 2012 at the RaBT-pass. Earlier data from 2007 to 2012 is therefore taken from the closest operational rain gauge, which is located in Inveruglas located approximately 9 km east of the pass (Fig. 1). The envelope representing the sequence of lowest data points that represent observed mass

movement at RaBT-pass is then considered as a minimum hydro-meteorological threshold condition. The threshold envelope is thus defined as:

$$T = R_0 - \alpha\left(\sum_{t=1}^{n} k^i \bullet r_i\right) \quad (1)$$

where T is the daily rainfall needed to initiate mass movement in mm; therefore, R_0 is the rainfall in mm needed to induce mass movement without antecedent precipitation. Here we assume that daily rainfall indeed contribute to triggering the mass wasting event although we do not know the exact time of the event compared to that day's rainfall. This might introduce uncertainty in our predictive model as discussed by Monsieurs et al. (2019). The regression coefficient α is derived from the slope of the envelope, and represents the reducing need of rainfall to initiate mass movement when the API increases. The API is the sum of rainfall of n days, where the reducing influence of days further away is governed by the factor k^i, which essentially represents the outflow of water from the regolith. This threshold allows calculation of the recurrence interval of hydro-meteorological trigger conditions at the RaBT-pass by dividing the total number of threshold exceedances by the total number of days in the available precipitation time series (Glade et al., 2000). Mass movement probability is determined by dividing the number of recorded events by the number of occurrences of threshold exceedance. Eq. (1) is applied to a rainfall time series spanning from 2007 to 2017 (Scottish Environmental Protection Agency, 2017), which includes the recorded mass movement events listed in Table 1.

3.2. Threshold application & scenario selection

The realisations of UKCP09 hydro-meteorological forecasts used for this study reflect the plausible responses of the atmosphere to the SRES A1B emission scenario, that are calculated on a global 300 kilometre resolution using the HadCM3 model and downscaled to 25 kilometre resolution using the Met Office Regional Climate Model (RCM) HadRM3 in eleven different configurations (Murphy et al., 2009; Table 2). The recurrence time of rainfall episodes that are able to facilitate mass movement can be determined for each configuration of the RCM, by identifying the amount threshold exceedances (T; Eq. (1)). As these configurations carry a degree of uncertainty (Harding et al., 2015; Murphy et al., 2009), as displayed by their climate sensitivity and average annual precipitation (Table 2), the selected critical rainfall episodes should cover the largest possible variation from the configuration ensemble in rainfall and API combinations capable of triggering mass movement at the study site. This selection of critical rainfall episodes is therefore based on the data points comprising the outline of the convex hull (Andrew, 1979) of the data points exceeding the established threshold from the ensemble of configurations. This sampling method effectively limits the number of simulations, yet covering the uncertainty imposed in the RCM configurations and providing insight in the effects of different precipitation regimes on mass movement hazard.

Table 2
Overview of Regional Climate Model (RCM) configurations, the resulting climate sensitivity (CS) in the HadRM3-model; and average annual precipitation (AAP) from 2017 till 2050.

RCM ID	CS (K)	AAP (mm)
x	3.53	2832.4
a	2.53	2836.0
c	2.82	2777.7
h	3.44	2872.6
i	4.40	2857.9
j	3.90	2759.4
k	4.44	2748.5
l	4.88	2865.3
m	4.54	2737.5
o	4.80	2682.8
q	7.11	2821.5

Sources: Hadley Centre for Climate Prediction and Research (2008); Christierson et al. (2012); Murphy et al. (2007).

3.3. CLiDE environmental modelling framework conceptual outline

To study the patterns in mass movement emerging from hydro-meteorological drivers, the CLiDE modelling platform is used, which comprises elaborate descriptions of geomorphological systems and processes (Barkwith and Coulthard, 2014). Moreover, CLiDE is capable of accurately quantifying hydrological processes, and the ensuing geomorphological processes, over a variety of spatial and temporal scales. This CLiDE platform is based on the integration of the Cellular Automaton Evolutionary Slope and River (CAESAR) model (Coulthard and Van de Wiel, 2006), Lisflood-FP (Coulthard et al., 2013; Bates et al., 2010) and the hydrological soil moisture module (Barkwith et al., 2015; Barkwith and Coulthard, 2014). The conceptual outline of CLiDE, which operates on a daily timestep, is illustrated in Fig. 4 and corresponds to row three in Fig. 3.

In the CLiDE modelling platform, precipitation is distributed between the atmosphere, surface water, the soil and groundwater using the SliM module. Subsequently, excess water is routed over the surface by the Lisflood-FP model (Bates et al., 2010). The ensuing fluvial transport of sediment through the modelling framework is governed by the CAESAR model. The non-fluvial sediment transport within CliDE comprises regolith diffusion, based on the slope gradient, and rapid mass movement. To trigger mass movements, CliDE uses an infinite slope model to evaluate the effects of hydro-meteorologically driven variations in effective stress (Selby, 1982; Barkwith and Coulthard, 2014). Failure is initiated when the stress of a portion of slope above a failure surface exceeds available shear strength. The subsequent runout is governed by the SCIDDICA-model (D'Ambrosio et al., 2003). In this cellular automaton, the dynamics of mass movement are governed by local interactions that govern the modification of the cell its substates. These interactions are coalesced in transition functions, which are applied during each time step. This results in dynamical behaviour of the described phenomenon. The substates represent physical characteristics and include: altitude; thickness and energy of landslide debris; depth of erodable soil cover; debris outflows. The importance of a number of these variables including soil or colluvium depth is still under discussion (Parker et al., 2016). The processes covered by the local interactions are: triggering, erosion and entrainment; debris outflows; update of debris

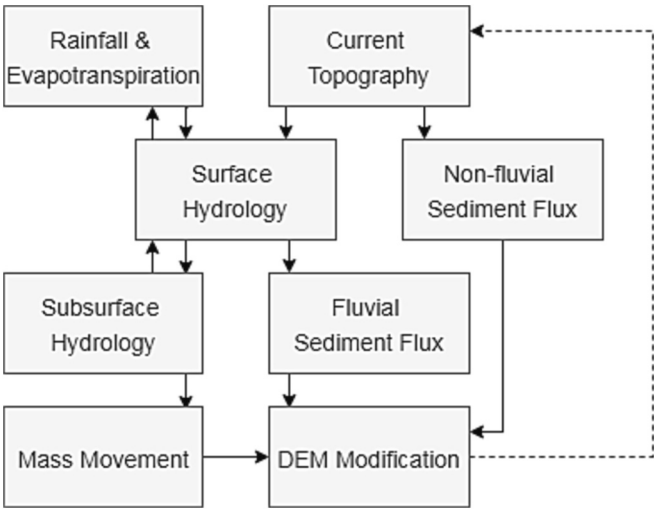

Fig. 4. Schematic overview of the covered processes in CLiDE Environmental Modelling Platform. Adapted from Barkwith et al. (2015). Note that the solid lines use data from the current time step and that the dashed line represents the start of a new timestep.

thickness and energy; and energy loss through frictional effects. Subsequently, the results of the independently simulated mass movement events are combined and averaged, yielding an average erosion or deposition and the associated variance based on the selected events. This allows identifying the dominant source areas at the pass. To gain more insight in the spatial distribution of the source areas and the underlying causes, the subsurface soil water depth at which the soil becomes unstable or 'critical soil water depth', is derived from the infinite slope model (stability Factor of Safety or *Fos* = 1) and its exceedances monitored during the simulations.

3.4. CLiDE input

The CLiDE modelling framework requires elaborate parameterisation (Table 3), including:

- Digital elevation model (DEM).
- Spatial distribution of depth to bedrock.
- Soil and bedrock properties (hydraulic conductivity; specific yield; soil friction angle; soil density).
- Initial hydrological conditions of soil and bedrock (initial soil water head, initial groundwater head, initial soil moisture deficit, initial near soil surface storage, potential evapotranspiration).
- SCIDDICA-model parameters (soil entrainment coefficient, frictional loss coefficient, adhesion coefficient, mobilisation threshold, initial debris thickness).
- Hydrological forcing through rainfall or surface water levels.

3.5. Soil & bedrock depth

The bedrock depth is derived from a transect that was logged by the British Geological Survey (BGS Landslide Team, 2018). The measured bedrock depth, slope angles and elevations are averaged to serve as input for a simplified exponential function (Appendix B). This function aims to extrapolate the measured bedrock depth over the study area as a function of slope angle (Pelletier and Rasmussen, 2009a; Heimsath et al., 2001) and elevation, which are both derived from a 5 metre digital elevation model (Intermap Technologies, 2007). Subsequently, spatially correlated noise was applied to the derived bedrock depth. Spatially correlated noise is applied to the generated bedrock depth to make the generated bedrock more representative of an irregular bed overlain by soil. The equation is presented in Appendix B. Additionally, a 1 *kyr* spin up was applied to generate a representative soil cover, comprising of soil production from bedrock Pelletier and Rasmussen (2009a) and diffusive soil transport (Appendix B Fig. B.1; Martin, 2000).

3.6. Soil texture & soil properties

The dominant soil groups are generally loam with significant silty or sandy components, using the NRCS-USDA classification system (Bown et al., 1982). All contain high silt contents ranging from 35 to 50 %. This classification is similar to the more recent assessments by Rayner and Nicoll (2012) who classify the dominant soils as sandy silt to silt loam. The characterisation of soil textures for this research uses these observations as a basis for the further development of a soil texture cover across the slope that encompasses the range indicated in Fig. 5.

Table 3
Overview of CLiDE input and its provenance (Barkwith and Coulthard, 2014).

Input	Source
DEM (5 m)	British Geological Survey (BGS Landslide Team, 2018).
Bedrock depth	Borehole data (BGS Landslide Team, 2018).
Soil properties	Balland et al. (2008); Prellwitz (1981); Morgan et al. (1998); Boorman et al. (1995).
Bedrock properties	Heath (1983); Morris and Johnson (1967).
Initial hydrology	Allen et al. (1998).

For sand and clay, an average texture fraction and standard deviation are defined and their fractions are calculated for each cell of the DEM, using Eq. (2) and Table 4:

$$T_{f,i}(x,y) = \mu_i(x,y) + \left(\sigma_{f,i} \bullet r_n(x,y)\right) \quad (2)$$

where $T_{f,i}(x, y)$ is the resulting fraction of texture class i, $\mu_i(x, y)$ is the predefined average fraction of texture class i, $\sigma_{f,i}$ is the standard deviation of texture class i and $r_n(x, y)$ spatially correlated noise. The residual texture fraction is considered to be silt. Furthermore, the organic matter in the topsoil is assumed at 7.5 % (Balzano et al., 2016). An overview of the soil texture distribution is shown in Appendix B.2 and Fig. B.2.

Pedo-transfer functions formulated by Balland et al. (2008), based on the soil textural distribution, soil organic matter and soil depth, are applied to estimate the relevant soil hydrological properties for three predefined soil layers, yielding a weighted average per cell. The top layer (ranging from 0 to 30 cm) includes 7.5 % organic matter, the second layer (from 30 to 100 cm) has an exponential decrease to zero in organic matter with depth and the base layer (from 100 to 150 cm) contains no organic matter. As CLiDE is a partly lumped parameter model, some distributed values have been averaged accordingly (Table 5).

Based on these values for the field capacity and wilting point, the hydrology of the soil type is classified as micro- porous with common bypass flow (Boorman et al., 1995). Furthermore, the soil is assumed to be at field capacity, based on the prevailing hydrological conditions (annual rainfall>3000 mm) and the assumption of a relatively even distribution thereof over the year. Hence, the initial soil moisture deficit and near soil surface store are both assumed to be zero. Although values for potential evapotranspiration can vary significantly over the year, an approximation of potential evapotranspiration of 1 mm day^{-1} is applied (FAO standards; Allen et al., 1998) for temperate regions with annual mean temperatures around 10 °C. Furthermore, since individual cycles of 9 days are simulated, the long-term effects of potential evapotranspiration are limited.

Because the dominant soil types are characterised by high hydraulic conductivities, it is reasonable to argue that the shear strength parameters of friction and cohesion can be assessed in terms of effective stress. The angle of internal friction for a soil column is calculated using the

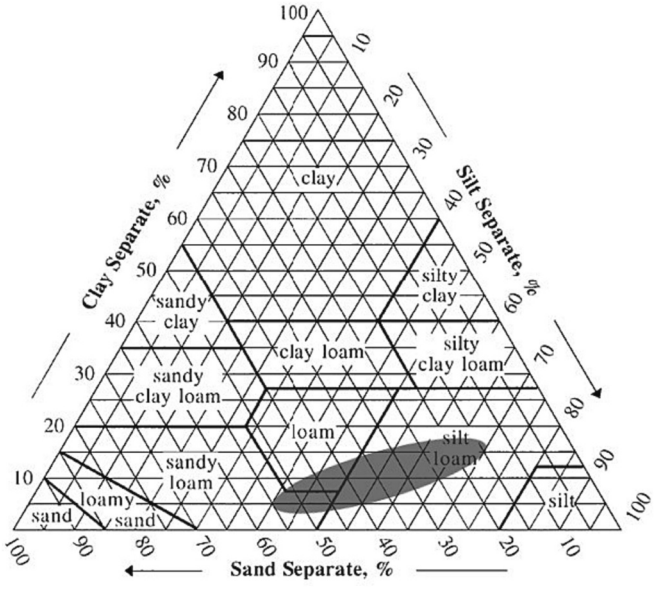

Fig. 5. NRCS-USDA soil texture triangle. The oval mark indicates the range in which the majority of the soil texture should vary.

Table 4
Mean and standard deviation per soil composite as applied in Eq. (2).

Soil texture	Sand (%)	Clay (%)	Silt (%)
μ_1	35.0	10.0	55.0
$\sigma_{f,t}$	15.0	5.0	15.8

Table 5
Averaged input parameters for CLiDE.

Parameter	Value
Hydraulic conductivity	0.26 m d^{-1}
Porosity	40 %
Field capacity	25 %
Specific yield	22 %
Parameter wilting point	8.4 %
Readily available water	21.6 %
Bulk density	1.55 mg/cm^3

relationships established by Prellwitz (1981), based on the texture and relative density of the soil:

$$cot\emptyset' = k_{\emptyset 1} - k_{\emptyset 2} \bullet D_r \quad (3)$$

where φ is the internal friction angle, $k_{\varphi 1}$ and k_2 are adjustment parameters, whilst D_r is the relative density of the soil. Table 6 shows the input parameters for Eq. (3). Consequently, the weighted average from the separate soil texture classes is the resulting effective friction, φ^j.

D_r is computed from Eq. (4) by means of the void ratios derived from the calculated porosities using Eq. (5) and the minimum porosity (E_{min}) and maximum porosity (E_{max}) assumed at 0.26 and 0.6 respectively (Prellwitz, 1981).

$$D_r = \frac{E_{max} - e}{E_{max} - E_{min}} \quad (4)$$

$$e_i = \frac{n_i}{1 - n_i} \quad (5)$$

For fine-grained soils it can be assumed that the effective cohesion is a function of the clay fraction. Therefore, a maximum value of 21 kPa for a clay fraction of 50 % (Morgan et al., 1998) is applied as at this point the matrix is already fully supported by the clay particles. The effective cohesion decreases linearly to zero with clay content.

The underlying bedrock is characterised by a hydraulic conductivity of 0.001 mm day^{-1} and a specific yield of 0.34 (Heath, 1983; Morris and Johnson, 1967). The bedrock is assumed to be saturated as the water from the bedrock is expected to have a minimal influence on the soil water regime, and thus mass movement initiation, due to the low conductivity and specific yield of the aquifer.

3.7. SCIDDICA

The input parameters used in the SCIDDICA-module are derived from the calibration as performed by D'Ambrosio et al. (2003). In this study, various debris flows from southern Italy were modelled. Their calibration was mainly based on the offset location of the flow as well as its end point. In a similar manner, the input parameters used to study the RaBT were calibrated to roughly approximate the 05-12-2015 mass movement event at RaBT. This event was used for calibration as offset location and the quantity of debris deposited on the A83 are relatively well documented. Table 7 shows the parameterisation of the SCIDDICA-module.

Additionally, the SCIDDICA-module requires prior identification of potential source areas. This reduces computational time as less nodes require evaluation. Consequently, potential source areas were identified for each rainfall episode, using an infinite slope model and a factor of safety approach ($FoS < 1$), using the soil water levels that were originated from the simulated episodes.

Table 6
Parameters resulting in the effective angle of internal friction from Eqs. (3) and (5).

Soil texture	φ^j (D_r = 100 %)	φ^j (D_r = 0 %)	$k_{\varphi 1}$	$k_{\varphi 2}$
Sand	33°	43°	1.54	0.0043
Silt	26°	36°	2.05	0.0067
Clay	15°	37°	3.73	0.0240

(Adapted from Prellwitz et al. (1994).)

4. Results

4.1. Hydrological thresholds

The API for the RaBT was calculated using 4, 8 and 12 antecedent days (n), for all months in which mass movements were recorded from 2007 to 2017 (Appendix Figs. A1, A2, A3). For these realisations, a value of 0.92 is assigned to the decay factor, k, in the API. The intercept with the y-axis denotes where a daily rainfall event could initiate mass movement. These values for $n = 4$, $n = 8$ and $n = 12$ are 71.2 mm, 61.3 mm and 57.1 mm respectively (Table 8).

This research aimed to evaluate the contributions of antecedent rainfall that conditions a slope and a daily rainfall amount that is required to trigger a mass movement. Our trials indicate that 8 antecedent rain-days provide the greatest consistency for the determination of a daily rainfall amount. Only one mass movement event (October 2007) fails to meet the established criteria. Hydrological conditions considered sufficient for initiating mass movements are met quite frequently without observed mass movement events. This could imply that no movement occurred, that an event was not registered, or that other factors outside the control of this research play a significant role. This could include, for example, slopes taking time to become prepared for failure. In some cases, once an event has taken place, the remaining slope material may occur in a state of tension that requires, for a period of time, a greater threshold for the initiation of further mass movements. Further research into these mechanisms fall outside the current scope of this study.

The recurrence interval of hydrological conditions capable of triggering mass movements is, on average, 49 days per year for the period of October 2007 to April 2012. When the threshold is applied to observations closer to the RabT for the period of April 2012 to December 2017, this recurrence interval increases to 67 days. Non-local precipitation observations therefore introduce significant uncertainty in establishing recurrence intervals. The number of events where hydrological conditions exceed the stability threshold is regarded as 'hits', and these are clearly more prevalent than the recorded events. For the period 2007–2012 there were 42 hits and only 3 recorded events giving a probability of occurrence of only 5 %. For the period 2012–2017 the probability of occurrence increases to 16 % (Table 9). It can therefore be concluded, logically, that local observations provide more relevant information, albeit still with a rather low degree of certainty.

4.2. Hydro-meteorological event selection for CLiDE

As shown in Fig. 6 the RCM forecasts show a wide variation in their

Table 7
Parameterisation of the SCIDDICA-module.

Parameter	Applied value
P_{adh}	0.01 m
P_f	0.1 m
P_r	0.1
P_{rl}	9 m
P_{mt}	$5m_2$
P_{er}	0.25

Table 8
Resulting constants and coefficients from fitting various values of n to Eq. (1):

	R_0	α	$\sum_{i=1}^{n} 0.92^i \cdot r_i$
T=	71.2	0.3014	$n = 4$
T=	61.3	0.1527	$n = 8$
T=	57.1	0.0981	$n = 12$

Table 9
Overview of number events of threshold exceedances of hydrological conditions (hits), recorded mass movement events; mass movement probability (P); and the recurrence intervals (RI) in days.

Dataset	Hits (days)	Events (days)	P (%)	RI (days)
2007–2012	42	3	4.76	49
2012–2017	31	5	16.13	67

response to climate change and the forthcoming hydro-meteorological trends. Especially in RCMs 'i', 'j' and 'l' much wetter conditions are forecast. The other RCMs mainly show an increase in recurrence time, which is likely to result in a reduction in mass movement frequency. Moreover, Fig. 7 shows the dominance of certain RCM configurations in the selection of hydro-meteorological events, which is shown in Fig. 7. Based on the convex hull of the threshold exceeding events in Figs. 7, 10 scenarios were extracted from the realisations of Table 2. The scenarios comprising the convex hull are selected as they cover conditions at the threshold plus a number of hydrological events representing the probable spread of extremes as generated by the RCM-driven hydro-meteorological forecasts. The selected rainfall episodes are shown Table C.1 (Appendix C).

4.3. Mass movement simulations

The critical soil water depth required to trigger slope movement is distributed rather uniformly across the slope but tends to increase in the valley bottom due to thicker soils and much gentler slopes close to 0°, as shown in Fig. 8A. Nonetheless, Fig. 8B shows that exceedance of critical soil water depths is largely restricted to areas below 500 metre altitude in the centre of the slope. The limited spatial extent of the unstable zones and their perpendicular position to the contour lines already indicate that gully formation and associated drainage patterns play a vital role in triggering mass movement in the study area. Additionally, the occurrence of some frequently unstable zones at higher elevations suggests that subsurface drainage patterns and accumulation in bedrock hollows can potentially mobilise material further up slope.

Source areas and subsequent runout of mobilised material are also largely constrained to gullies, as shown in Fig. 8C. The relatively low variance of erosion and deposition in the centre of the slope, shown in Fig. 8D, implies that these gullies experience erosion during mass movement events and thus are the main source or transport areas. Examination of the individual simulations in Appendix D (Fig. D.1) confirms this interpretation but also shows that different antecedent precipitation patterns can mobilise different areas and runout paths. Wetter episodes or episodes with more concentrated precipitation, such as the 21-11-2032, 20-12-2036 and 21-10-2038 scenarios, mobilise material up to 700 metre elevation. This results in some low variance areas in the southern parts of the slope as well as at higher altitudes.

5. Discussion

The model outcomes provide an accurate representation of field observations and slope features visible in Fig. 2. The source areas pathways of mass wasting coincide effectively with the gullies observed at the study site and confirm that these are key factors in the hill slope its evolution both short term and long term. Moreover, the depositional areas down slope correspond accurately with the transport corridor at the study location. Altogether, this shows that although some limitations of the model framework and input parameters could be studied in further detail, such as the daily timestep for rainfall influx and impacts of hill-slope-scale features on future precipitation regimes, the

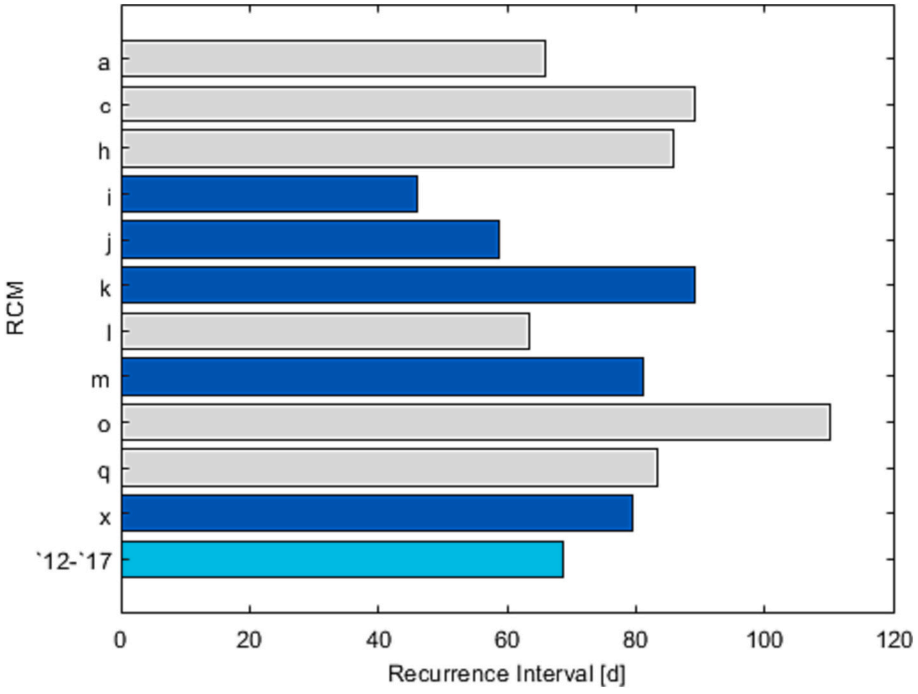

Fig. 6. Recurrence intervals of hydrological threshold exceedance. In light blue the recurrence interval is shown for the data collected from 2012 and 2017. Grey and dark blue shading show recurrence per RCM (Regional Climate Model) configurations of Table 2. RCM I, j and l indicate to wetter conditions and increased risk for mass movements. Dark blue shading present the RCM configurations used for the hydro-meteorological simulations.

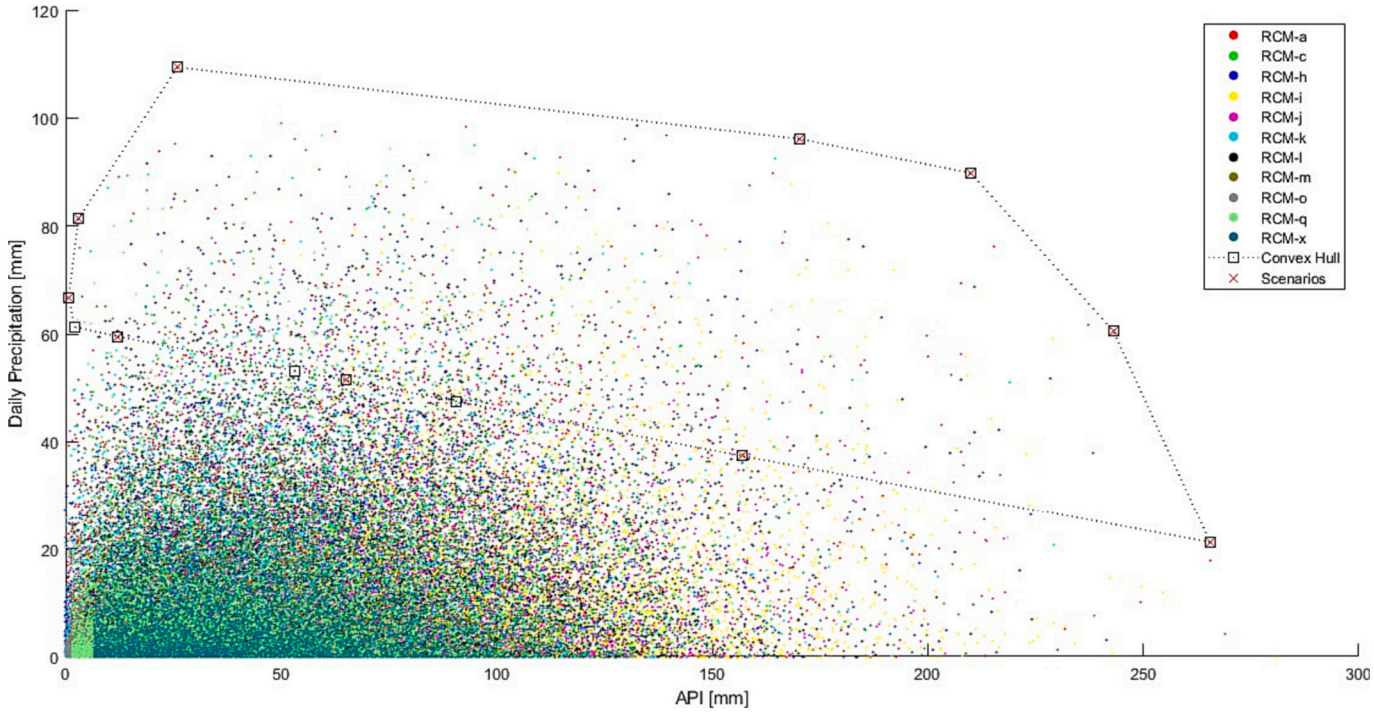

Fig. 7. Daily precipitation plotted against the antecedent precipitation index (API) for all Regional Climate Model (RCM) realisations. The convex hull shows the critical rainfall episodes used for the scenarios. Table 2 presents information about the RCM configurations and the corresponding RCM-IDs.

methodologies set out in this study provide a robust basis for studying and modelling the effects of future climate change on hill slope processes and evolution.

5.1. Hydrological thresholds

Ballantyne (2004) reported 24-hour thresholds of 60 mm to 80 mm for initiating mass movement in the Scottish Highlands, which is in line with the results of the established hydrological thresholds. The results reported by Pennington et al. (2014) and Chen et al. (2018) indicate a strong correlation between mass movement in these environments and antecedent precipitation based on seven days. Generally, the slopes at the RabT respond quickly to changing precipitation conditions. This study therefore assumes that thresholds based on four or eight antecedent days are relevant for the study site with eight antecedent days at the extreme end to generate relations with mass movement occurrence. These thresholds can then be used to calculate recurrence times using UKCP09 forecasts. The results can then provide important inputs into the design of early warning systems and mitigation. Furthermore, this method can be applied over a number of temporal scales (Dahal and Hasegawa, 2008) and has been applied widely in numerous environments (Glade et al., 2000).

When attempting to segregate mass movement events from the continuous precipitation dataset, it is evident that threshold exceedance does not necessarily trigger mass movement. The lack of mass movement, despite surpassing threshold values, can likely be attributed to a shortage of material available for entrainment due to previous events (Brayshaw and Hassan, 2009) or to insufficient rainfall intensities (Sparkes et al., 2017). Moreover, events that had limited impact on the transport route are likely less well-reported and might cause gaps in the data. Also the development of reporting technologies, both in-situ and after events, has the potential for more elaborate and accurate coverage of events at the pass. Subsequently, the limited thirteen event database used for this study could be expanded, which would be beneficial for improving defined thresholds and the mass movement probability shown in Table 9.

One mass movement event was recorded whilst the threshold was not surpassed. This particular case (28 October 2007) could have been caused by prior dry conditions, which is suggested by the relatively low observed APIs in figure A2This might have caused reduced suction between particles (Estabragh et al., 2017) and preferential flow in the soil (Sun and Cui, 2018). Moreover, the rainfall data was measured approximately 10 km away. Due to the localised nature of precipitation, especially in mountainous regions (Cosma et al., 2006), hydro-meteorological differences could be substantial on small spatial scales (Faurès et al., 1995).

Further improvement in segregating the mass movement events from the data series could be achieved by deducting the decay factor, applied in the calculation of the API, from regional hydrographs (Klaassen and Pilgrim, 1975; Smakhtin and Masse, 2000). However, this requires a gauged catchment for calibration purposes, which was not available for the study site. Additionally, exponential or polynomial thresholds can be established but data scarcity would initiate errors, mainly when dealing with extremities in the data.

5.2. Future mass movement hazard

When comparing the historic data to the recurrence intervals of mass movement facilitating conditions in the UKCP09 forecasts (Fig. 6) only three hydro-meteorological forecasts (i, l and j) yield lower recurrence intervals than the observed 67 days for the historical data (2012–2017). The general reduction in mass movement frequency in the majority of the forecasts coincides with drying of the study area and subsequent lowering of the observed APIs. This is supported by trends that have been observed for other hydrological applications using the UKCP09 datasets (Christierson et al., 2012; Sanderson et al., 2012; Kay and Jones, 2012). The main findings of these studies emphasise the aggravating hydrological differences between the seasons as shown in Fig. 9.

However, this does not imply that mass movement hazard at the pass is likely to decline. As shown by Sanderson (2010), extreme precipitation events are forecast to increase, especially during autumn/winter. It is also likely that convective summer storms are likely becoming more

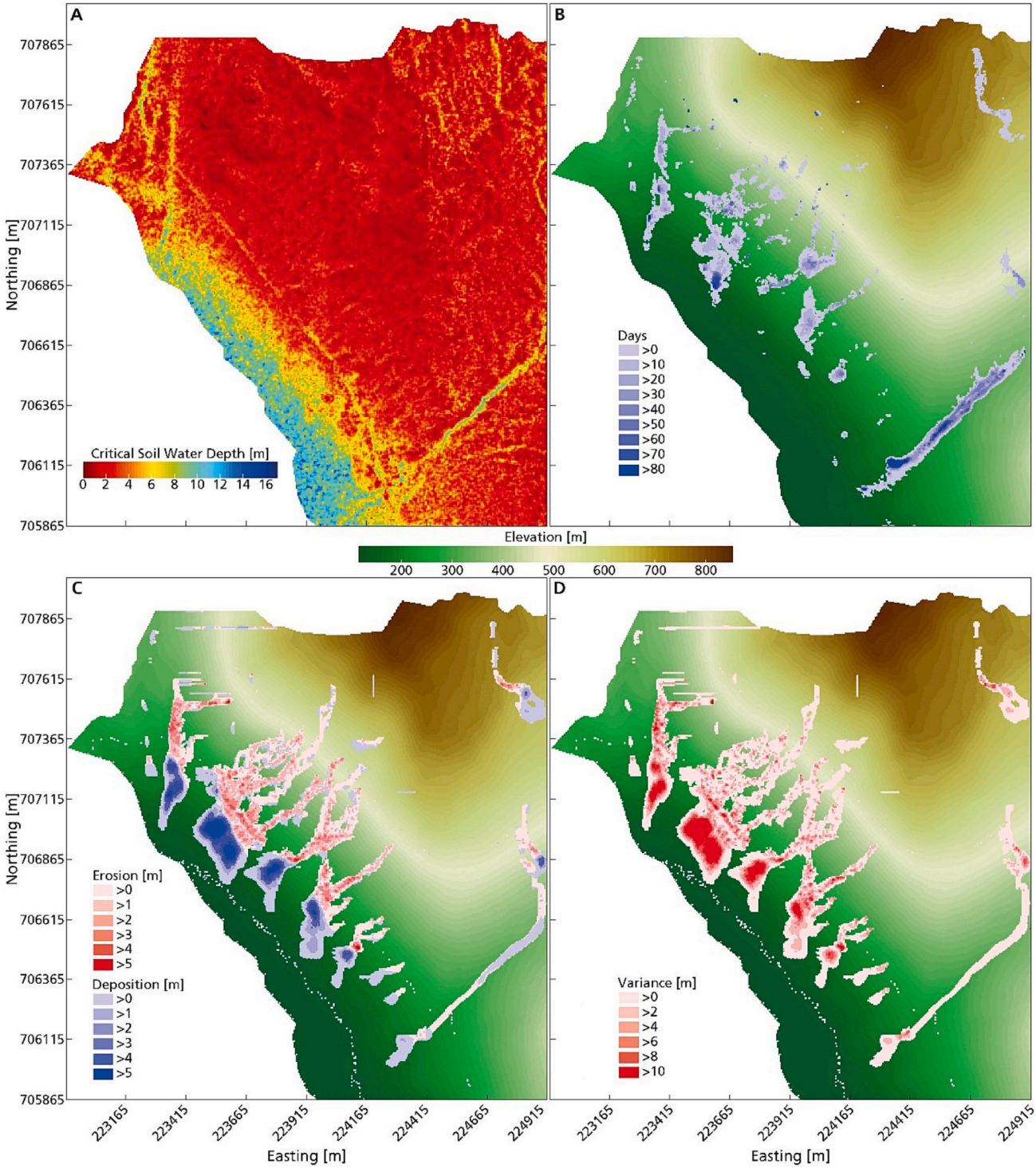

Fig. 8. Summary of the 10 simulated mass movement scenarios listed in Appendix C1. Maps of the individual scenarios are shown in Appendix D. Here A) shows the critical water depth and B) illustrates that exceedance of critical water depth occurs mainly at lower locations on the slope, C) shows erosion sites (sources of material) and where the material is deposited whilst D) illustrate the variance of the 10 simulations.

severe and thus, despite an increase in recurrence interval, the magnitude of mass movements will potentially increase (e.g. Chan et al., 2018). For instance, RCM's k, m and x indicate an increase in recurrence intervals. However, these are also frequently captured by the convex hull. This might suggest that the magnitude of events is more extreme regardless of these scenarios receiving less precipitation. In turn, this can be attributed to more concentrated events. Contrarily, when comparing the current annual average precipitation (3180 mm between 2007 and 2017) with those in Table 2 it is evident that all RCM scenarios experience drying, yet some show lower recurrence intervals, which stresses the importance of changing precipitation regimes. Besides the implications of these changing regimes, prolonging droughts can also have significant effects on slope stability (Chertkov, 2002; Van Asch et al., 2009; Sun and Cui, 2018). Additionally, the occurrence of mass wasting and subsequent removal of source material might impact the required influx of rainfall and its intensity for new mass wasting on that particular

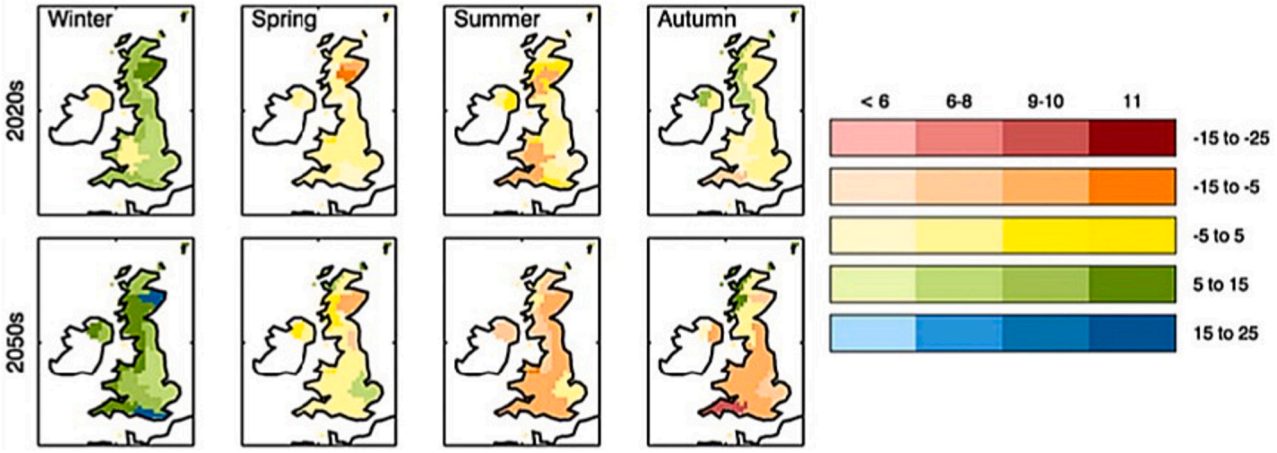

Fig. 9. Projections for the percentual change in mean runoff up to the 2050's compared to 1961–1990, following from the UKCP. Note that the four possible shadings of the colour indicate the extent of agreement between the RCM realisations and the multi-model mean.
Adapted from Sanderson et al. (2012).

location (Parker et al., 2016). This should thus be considered when evaluating specific locations rather than the full scale of the hill slope.

When comparing the landslide inventory (Table 1) with the convex hull selection, it is evident that there are similarities. Both are dominated by autumn/early-winter events (September–December). The data points selected by the convex hull can be considered outliers, but as mass movement occurrence is primarily driven by low confidence extremities, it appears that this approach reflects the historic inventory very well (Kirschbaum et al., 2012). The epistemological and ontological assumptions in climate models introduce major uncertainties in the resulting climate forecasts (Foley, 2010). These uncertainties mainly originate from sub-grid-scale processes (Holmes et al., 2017). Nonetheless, the findings of Otto et al. (2018) suggest that extreme events, such as the 2015 storm Desmond which triggered mass movement at RaBT (Sparkes et al., 2017), are likely to occur more frequently under climate change. Therefore, the inclusion of outliers in the evaluated rainfall episodes is necessary to more comprehensively evaluate the range of slope dynamics in this region.

5.3. Mass movement simulations

The dominant source areas are mainly restricted to areas between 300 and 500 metre elevation in the centre of the slope. Here, a small concavity-convexity transition causes water either to stagnate in the convex hollows or to be forced through thinner soils, as shown in Fig. 10b, increasing pore pressures and thus causing slope instabilities. Also, the confinement of water by the present gullies and the coinciding subsurface drainage channels (Fig. 2) contributes to triggering of mass movement and the entrainment of gully floor deposits, as shown conceptually in Figs. 8 & 10. As such, it is shown that soil types and heterogeneities in their properties seem to play a marginal role in activating mass movement at the study site.

Different precipitation regimes with similar APIs have shown to mobilise different source areas, which stresses their importance for mass movement hazard (Ng et al., 2001; Tsai, 2008). Moreover, under persistently wetting regimes ($API > 200$ mm) material up to 700 metre altitude is mobilised. Under such precipitation regimes only limited drainage can occur and the subsequent saturation of the soil can trigger mass movement, for instance through the collapse of pipe systems. Consequently, wetter or aggravating climate change scenarios, which will experience higher APIs during mass movement events, are likely to mobilise material further upslope than is currently the case at the RaBT pass. Localisation of the main source areas and runout paths, as well as their response to changing precipitation regimes, is especially valuable during the evaluation and implementation of maintenance and

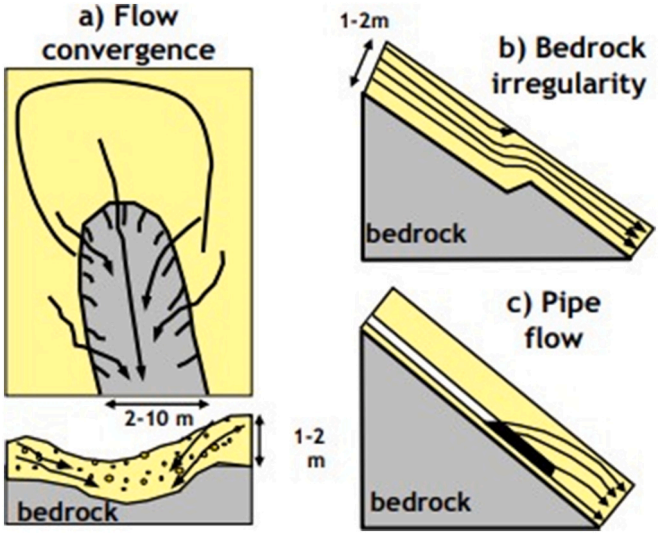

Fig. 10. Conceptual overview of the main causes of mass movement through surface and subsurface flow on hill slopes covered by shallow soils. Adapted from Crosta and Frattini (2001). The model simulations shown in Fig. 8 match well with these conceptual process illustrations.

operation strategies, that aim to prevent disruption of transport services along the A83.

Although included in the selection, three out of the ten simulations did not result in mass movement, which were mainly simulations with little antecedent precipitation. Hence it is likely that surface runoff that entrains material following high intensity rainfall peaks (Van Asch et al., 1999; Kean et al., 2013) is influential at the study site (Sparkes et al., 2017). This implies that the current methodology, which applies the infinite slope model and operates on a daily timestep, can overlook this process. Together with expected implication of changing precipitation regimes discussed in Section 4.2, this suggests that modelling at smaller temporal scales is likely to provide better understanding of the response of the RaBT slopes to different precipitation regimes.

6. Conclusions

Meteo-hydrological conditions are the main trigger for mass movement in many environments. Consequently, alterations of the hydrological cycle through climate change will have strong consequences on

the frequency and severity of mass movement. This has implications for adaptation and mitigation measures, and the corresponding costs, to cope with future hazard. To recognise current and future hazard, it is necessary to understand, quantify and evaluate the hydrological components essential in mass movement triggering. Hence, this study addresses the main spatial and temporal implications for mass movement through climate change at the RaBT pass.

The deduction of a rainfall threshold for mass movement triggering, based on the daily precipitation and antecedent precipitation index, resulted in: $T = 61.3 - 0.1527 * API$ ($n = 8$). Its subsequent application to UKCP09 forecasts suggests that mass movement frequency is likely to decline at the study site. This can mainly be attributed to aggravating differences between seasons. However, various studies emphasise the concentration of precipitation in fewer events as a result of climate change, and mass movement severity is likely to increase.

The rainfall scenarios selected from the ensemble of UKCP precipitation forecasts, by means of a convex hull method, were applied in CLiDE. Although converging flow in gullies mainly governs mass movement triggering, a distinct response of the dominant source areas to antecedent precipitation was observed. Normally situated between 300 and 500 metre altitude, the source areas migrated up slope to 700 metre altitude under wetter conditions.

These results could be used to bridge the gap between studies that focus on different components of mass movement hazard such as: direct observations of the RaBT pass and quantification of specific events (Sparkes et al., 2017; Bainbridge et al., 2018; Balzano et al., 2016); the implications of climate change on hydrological trends in the United Kingdom (Christierson et al., 2012; Murphy et al., 2007, 2009); and adaptation and mitigation practices (Macklin, 2013; Rayner and Nicoll, 2012; McQuaker et al., 2014). Moreover, these findings can contribute to the cost-effective implementation of various adaptation and mitigation practices. Especially environmental engineering practices, such as revegetation, barrier placement and the installation of early warning systems (McQuaker et al., 2014; Bainbridge et al., 2018; Rayner and Nicoll, 2012), can benefit significantly from the identification of the main source areas and potentially hazardous precipitation regimes. Furthermore, the methodology conveniently reduces the computational load of the evaluation of the applicability of such practices in various climate change scenarios.

This paper describes a pathway for the analysis of mass movement at RaBT, but it is aware of the large number of assumptions that had to be made in the absence of good, reliable data. In order to enhance input parameter quality and relevance of the model to reality it is recommended to carry out further engineering geomorphological studies, particularly regarding the characterisation of the heterogeneity of slope materials and depth to bedrock fluctuations (see e.g. Finlayson, 2020). The continued gathering and sharing of good quality observational data (e.g. climate, soil properties, multi-temporal topographical data) will further enhance future modelling capabilities at this important site.

Declaration of competing interest

The authors declare that they have no known competing financial interests or personal relationships that could have appeared to influence the work reported in this paper.

Data availability

Data will be made available on request.

Acknowledgements

The authors would like to acknowledge the British Geological Survey and especially its Landslide Team for their guidance and sharing of data. Furthermore Mr. Gareth Jenkins is gratefully thanked for his contributions to visualisations of the study site. A significant contribution to this research comes from the Scottish Environmental Protection Agency, in particular form Ms. Helen James. She has been of great help with respect to obtaining the rainfall data extensively used in this study. We are grateful to the staff of the Graphic Design department for their help with the illustrations.

Appendix A

A.1. Thresholds

Three figures presenting daily precipitation plotted as a function of the antecedent precipitation index (X-axis), based on 4, 8 and 12 antecedent days (Y-axis), for the complete dataset from 2007 till 2017. Blue circles refer to the dataset of 2007–2012, red circles to the 2012-2017 dataset (Table 9). The intercept of the dashed line on the Y-axis when daily rain could initiate mass movements.

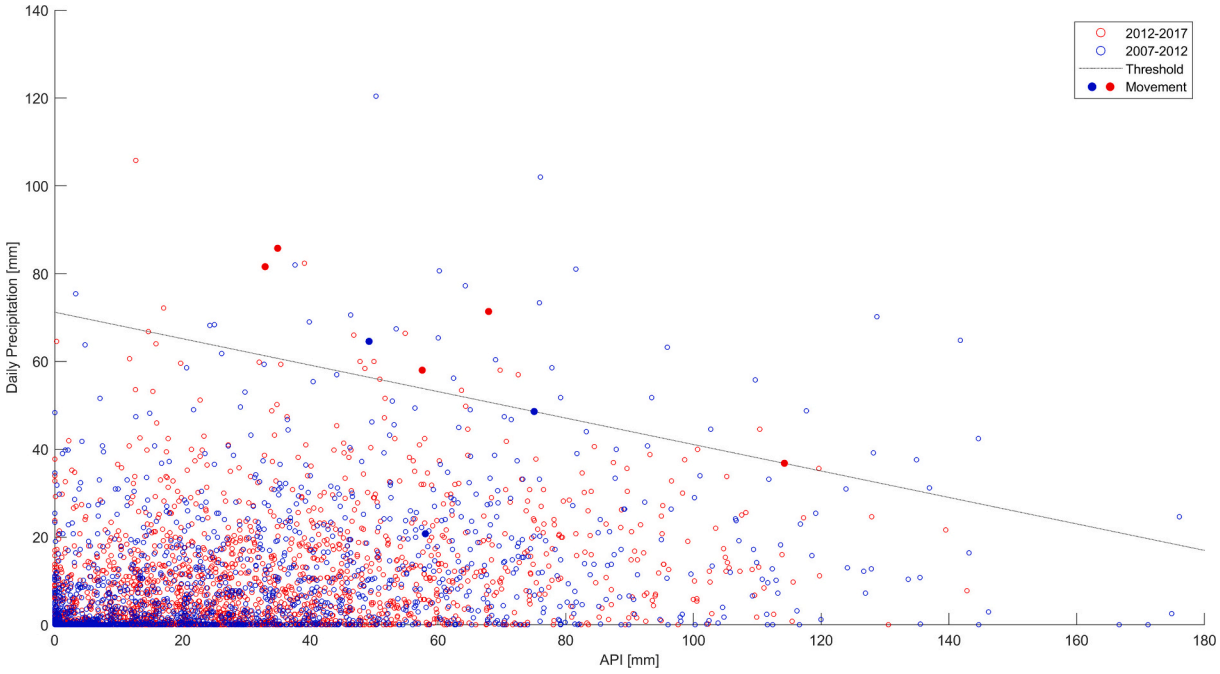

Fig. A1. Daily precipitation plotted as a function of the antecedent precipitation index, based on 4 antecedent days, for the complete dataset from 2007 till 2017.

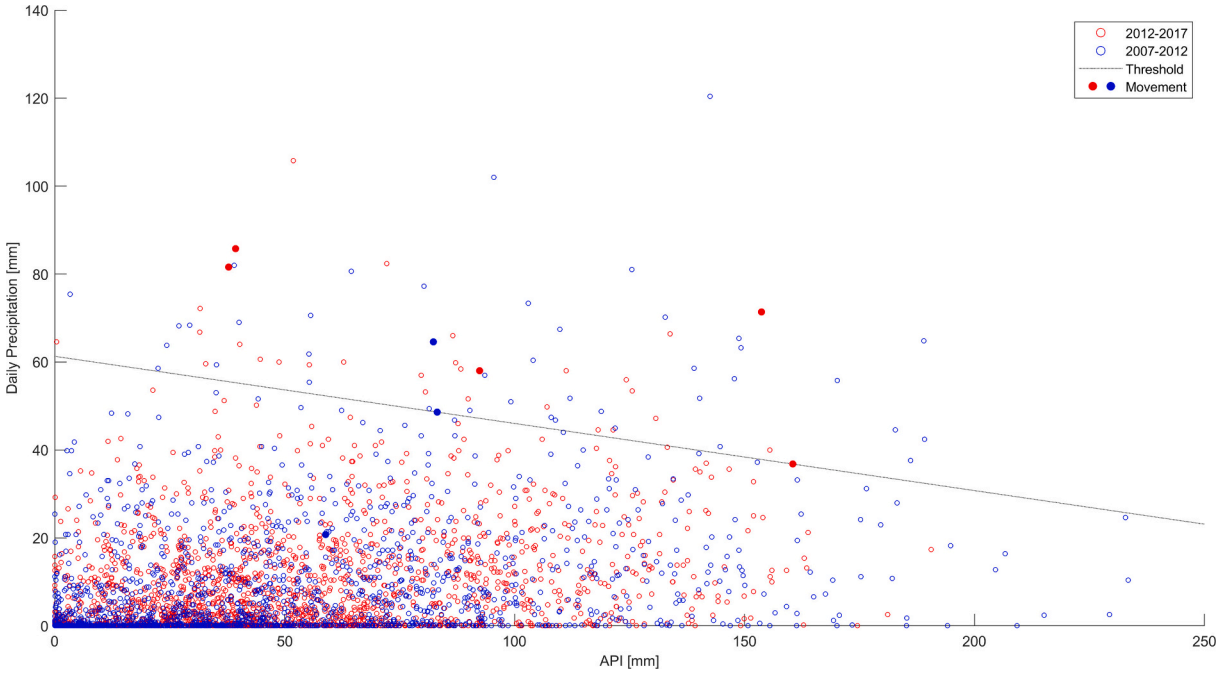

Fig. A2. Daily precipitation plotted as a function of the antecedent precipitation index (X-axis), based on 8 antecedent days (Y-axis), for the complete dataset from 2007 till 2017.

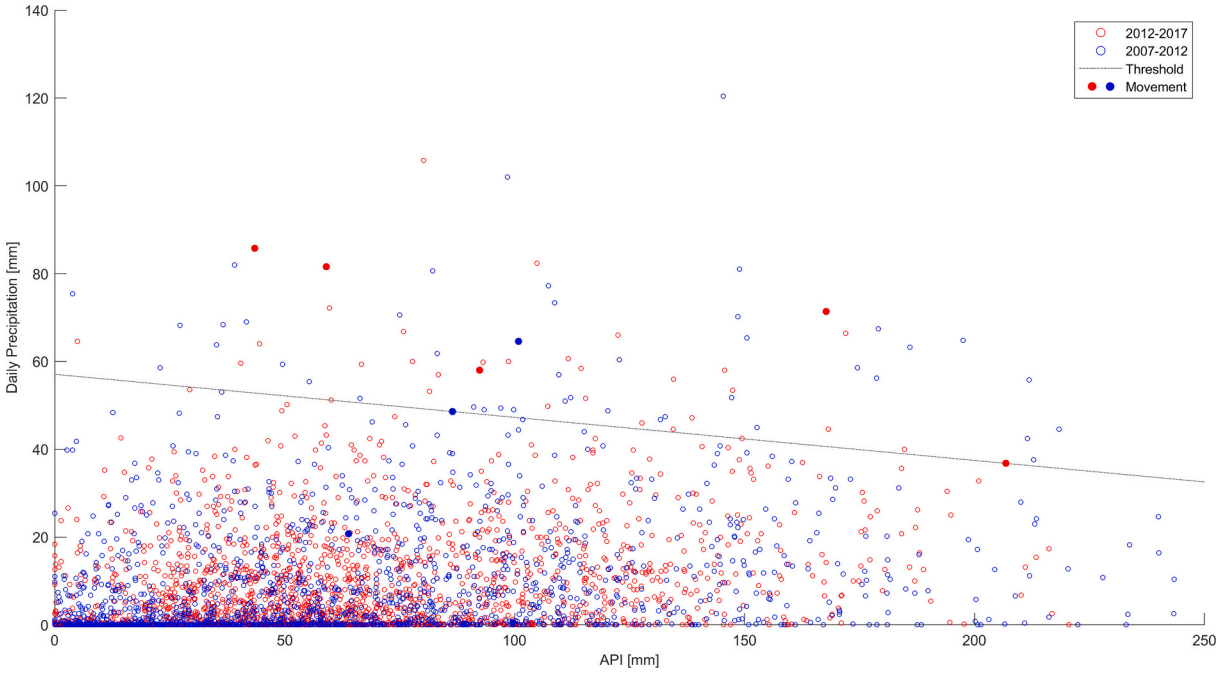

Fig. A3. Daily precipitation plotted as a function of the antecedent precipitation index, based on 12 antecedent days, for the complete dataset from 2007 till 2017.

Appendix B. Parameterisation

B.1. Bedrock depth

The bedrock depth was derived from the original digital elevation model using:

$$B_i(x,y) = Z(x,y) - \frac{D_1 cos\beta(x,y)}{Z(x,y)^{D_2}} \tag{6}$$

where B_i is the initial bedrock depth, Z is the surface elevation in metres, D_1 and D_2 are empirical scaling parameters and β is the slope angle. The empirical parameter D_1 is derived from solving Eq. (6) for the averaged values 216 m for the bedrock elevation; 25.5° for the slope angle; 221 m for the surface elevation; and $D_2 = 1$. Consequently, a value of 1257 m is applied for D_1. The introduction of D_2 as 1.12, was thought to be necessary to realise a stronger decrease of the soil cover upslope. To make the generated bedrock more representative of an irregular bed overlain by soil, spatially correlated noise is applied to the generated bedrock depth, using Eq. (7).

$$B_{n(x,y)} = B_i(x,y) + r_n(x,y) \tag{7}$$

where $B_{n(x,y)}$ is the new bedrock, $B_i(x, y)$ the originally derived bedrock and $r_n(x, y)$, a random number from a normal distribution (0,2). To make the noise spatially correlated, the numbers in r are filtered using the Moore grid and fractional contributions shown in Eq. (8).

$$r_n(x,y) = \sum \begin{bmatrix} r(x-1,y-1) & r(x,y-1) & r(x+1,y-1) \\ r(x-1,y) & r(x,y) & r(x+1,y) \\ (r(x-1,y+1) & r(x,y+1) & r(x+1,y+1) \end{bmatrix}^{\circ} \begin{bmatrix} 0.0251 & 0.1453 & 0.0251 \\ 0.1453 & 0.3183 & 0.1453 \\ 0.0251 & 0.1453 & 0.0251 \end{bmatrix} \tag{8}$$

In the subsequent spin up, the soil production is modelled using Pelletier and Rasmussen (2009a), in which a characteristic soil depth parameter of 0.5 m (Heimsath et al., 1997) is applied. The findings of Pelletier and Rasmussen (2009b) for granite suggest a potential production rate of approximately 0.00025 m yr^{-1}, assuming a mean annual temperature of 9.5 °C and a mean annual precipitation of 2000 mm. However, to account for the bedrocks schistosity (Marui and International Research Society Interpraevent, 2006), an enhanced maximum potential production rate of 0.0003 m yr^{-1} is assumed. To redistribute the produced soil material through the system, diffusive transport is introduced through Eq. (9) (Martin, 2000)

$$Q_s(x,y) = -D_e \left[\frac{\delta Z}{\delta x} + \frac{\delta Z}{\delta y} \right] \tag{9}$$

Here Q_s is the soil flux in $m^3 \cdot t^{-1}$, D_e is the erosive diffusion in $m \cdot t^{-1}$ and dZ/d(x,y) the change of elevation in the x- and y-direction. Within the spin-up, the erosive diffusion is based on the rate of soil creep as discussed by Kirkby (1967) and a rate based on frequent landslide activity by Martin (2000) yielding an erosive diffusivity of 0.1002 $m \cdot yr^{-1}$.

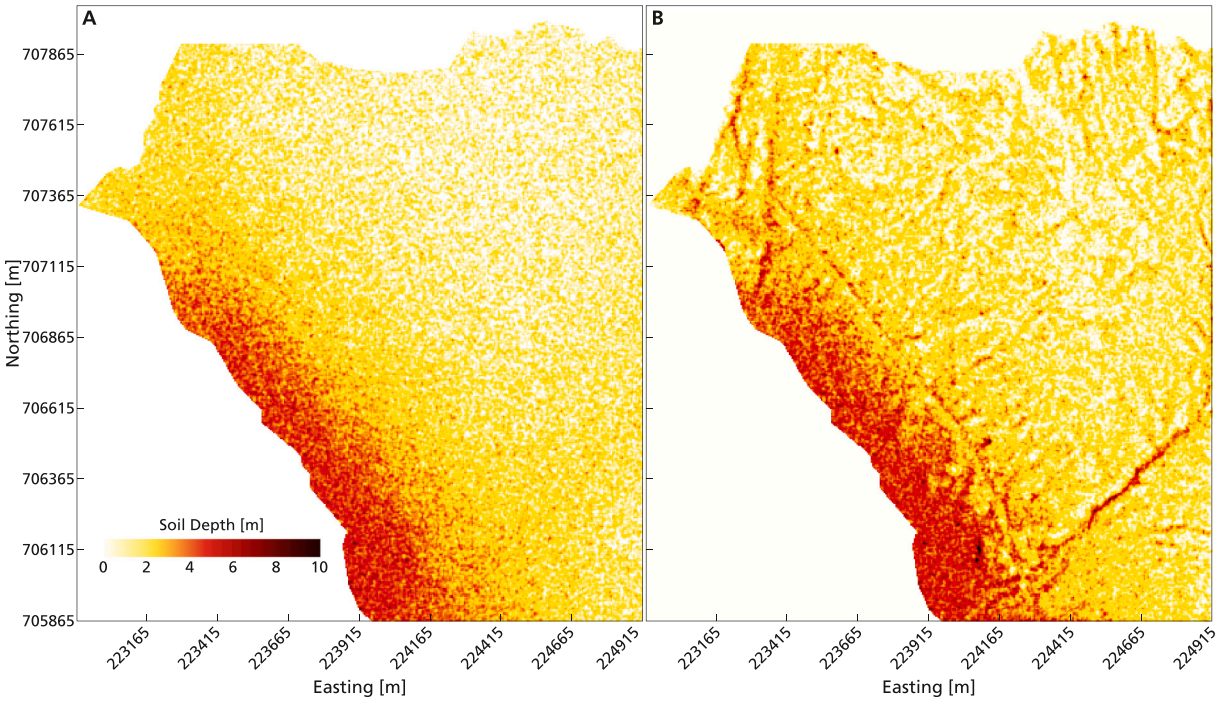

Fig. B.1. Overview of the simulated soil development over time. (A) Initial soil depth. (B) Soil depth after 1 kyr soil production Pelletier and Rasmussen (2009a) and diffusive transport Martin (2000).

B.2. Soil texture

Similar to the bedrock, the soil texture fractions are subject to spatially correlated noise. A similar procedure is therefore applied to the soil texture fractions, where r_n consists of a random number from the standard normal distribution (0,2). The soil texture is assumed to be more spatially correlated than the bedrock depth. Hence an increased radius of two cells in the Moore grid is applied to filter the numbers in r_n (Eq. (8)).

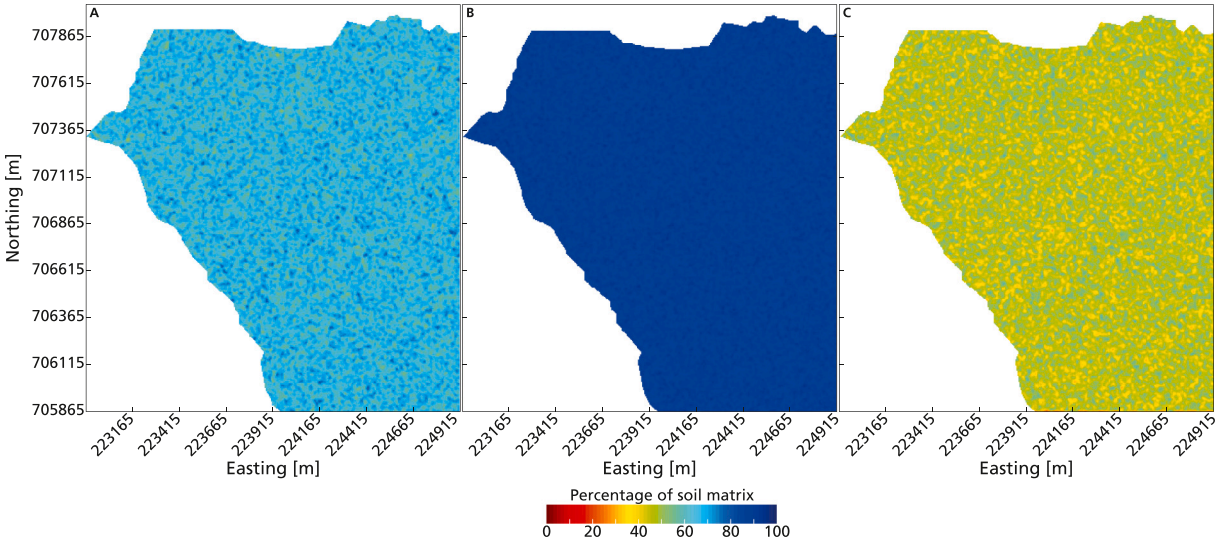

Fig. B.2.

Fig. B.2 shows the soil texture distribution as applied in this study, which results from the methods described in Section 3.6. A) Sand content; B) clay content; C) silt content.

Appendix C. Precipitation scenarios

Table C.1
Overview of selected scenarios (Table 2); the governing regional climate model (RCM); the associated daily precipitation regimes for days 1 (r1) to 8 (r8); the subsequent antecedent precipitation index (API).

RCM	r_8	r_7	r_6	r_5	r_4	r_3	r_2	r_1	API	Precipitation	Date
k	0.1 mm	0.1 mm	0 mm	0 mm	0 mm	0.1 mm	0 mm	3 mm	2.94 mm	81.30 mm	23-11-2019
k	0.4 mm	0.9 mm	0 mm	0 mm	0.1 mm	0 mm	0 mm	0 mm	0.71 mm	66.60 mm	05-03-2022
m	12.4 mm	0 mm	0.1 mm	6.3 mm	20.8 mm	12.9 mm	0.7 mm	3.9 mm	25.95 mm	109.40 mm	23-01-2024
i	5.8 mm	26.7 mm	17.2 mm	68.6 mm	25.2 mm	14.7 mm	15.5 mm	12.9 mm	156.87 mm	37.40 mm	24-09-2028
j	52.6 mm	46.2 mm	4.3 mm	1.5 mm	2.3 mm	6.4 mm	48.2 mm	96.8 mm	209.97 mm	89.80 mm	21-11-2032
x	4.1 mm	3.6 mm	36.7 mm	14.9 mm	27.2 mm	68.3 mm	7.8 mm	73.6 mm	170.35 mm	96.10 mm	18-12-2036
x	36.7 mm	14.9 mm	27.2 mm	68.3 mm	7.8 mm	73.6 mm	96.1 mm	34.3 mm	265.52 mm	21.20 mm	20-12-2036
m	12.9 mm	43.8 mm	9.7 mm	18.8 mm	58.5 mm	10.4 mm	4.8 mm	2.5 mm	64.93 mm	51.40 mm	27-10-2037
j	22.5 mm	12.8 mm	31.3 mm	25.6 mm	49.6 mm	47.5 mm	89.7 mm	61.8 mm	243.07 mm	60.50 mm	21-10-2038
k	0.1 mm	0 mm	0 mm	0.4 mm	15 mm	0.7 mm	3.7 mm	3.6 mm	12.10 mm	59.50 mm	31-12-2044

Appendix D. Simulation of erosion and deposition for selected future scenarios

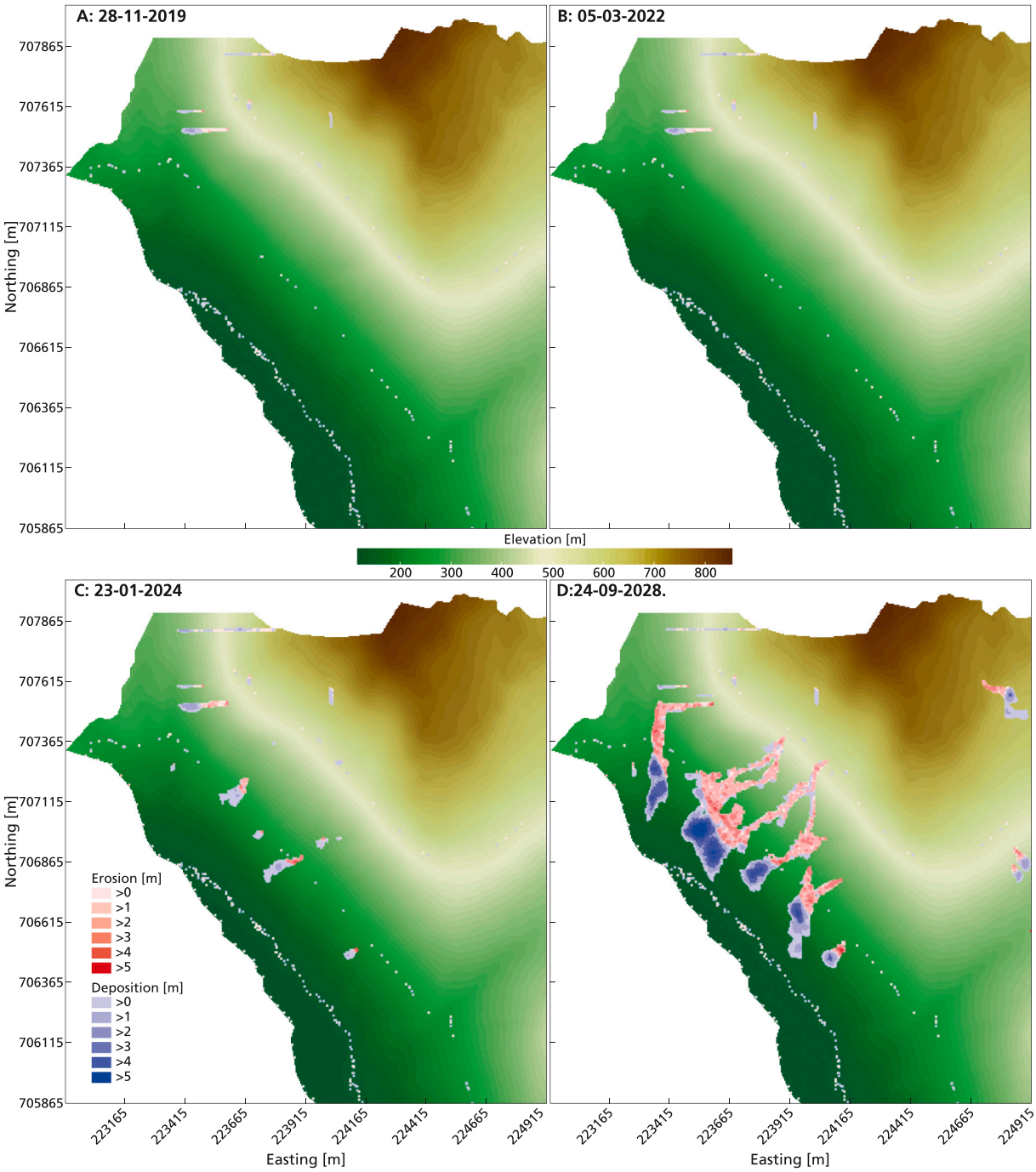

Fig. D.1. Resulting erosion and deposition patterns from the scenarios depicted in Table C.1 until the year 2044. The simulation dates are indicated in the upper-left corner.

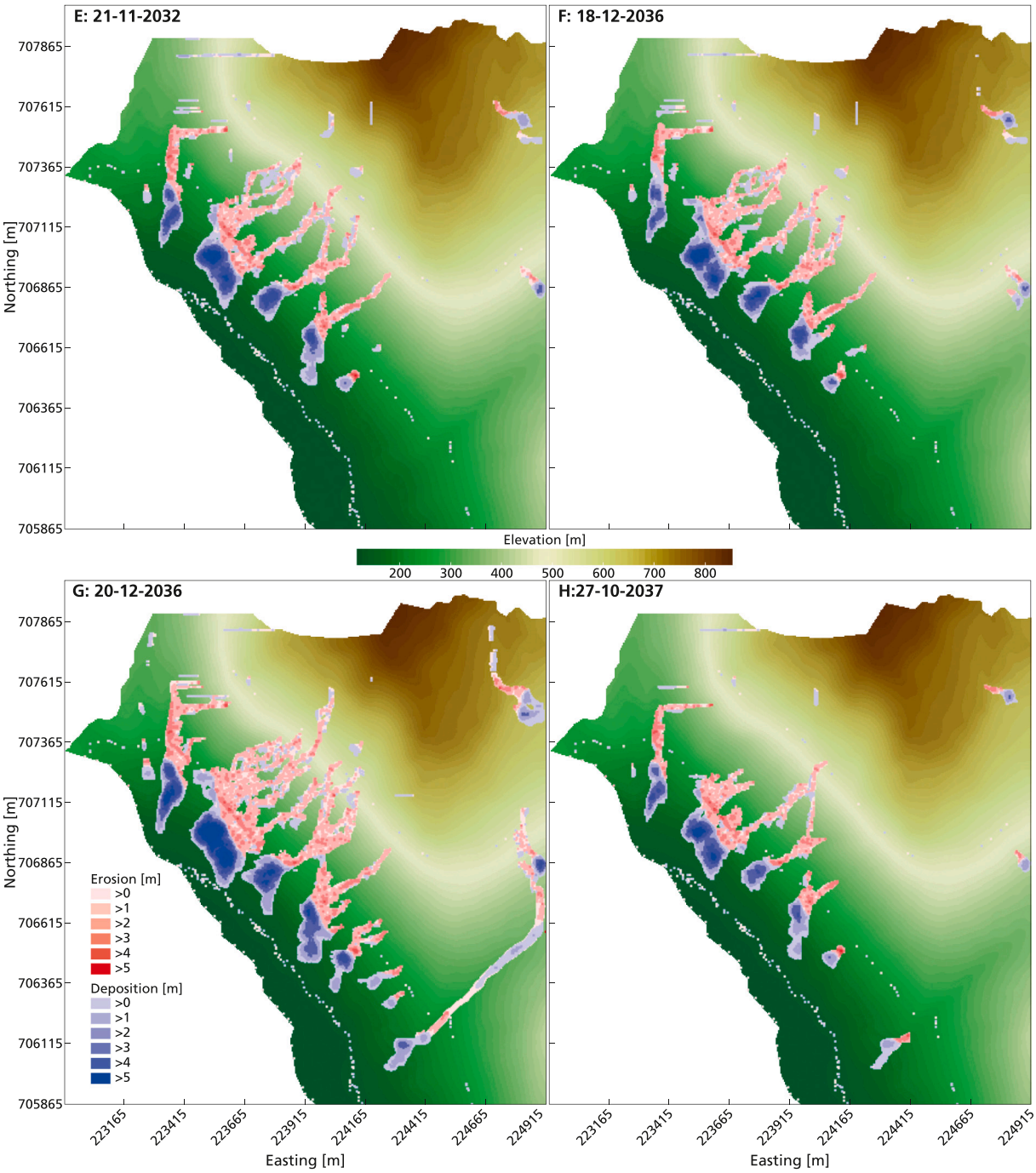

Fig. D.1. (*continued*).

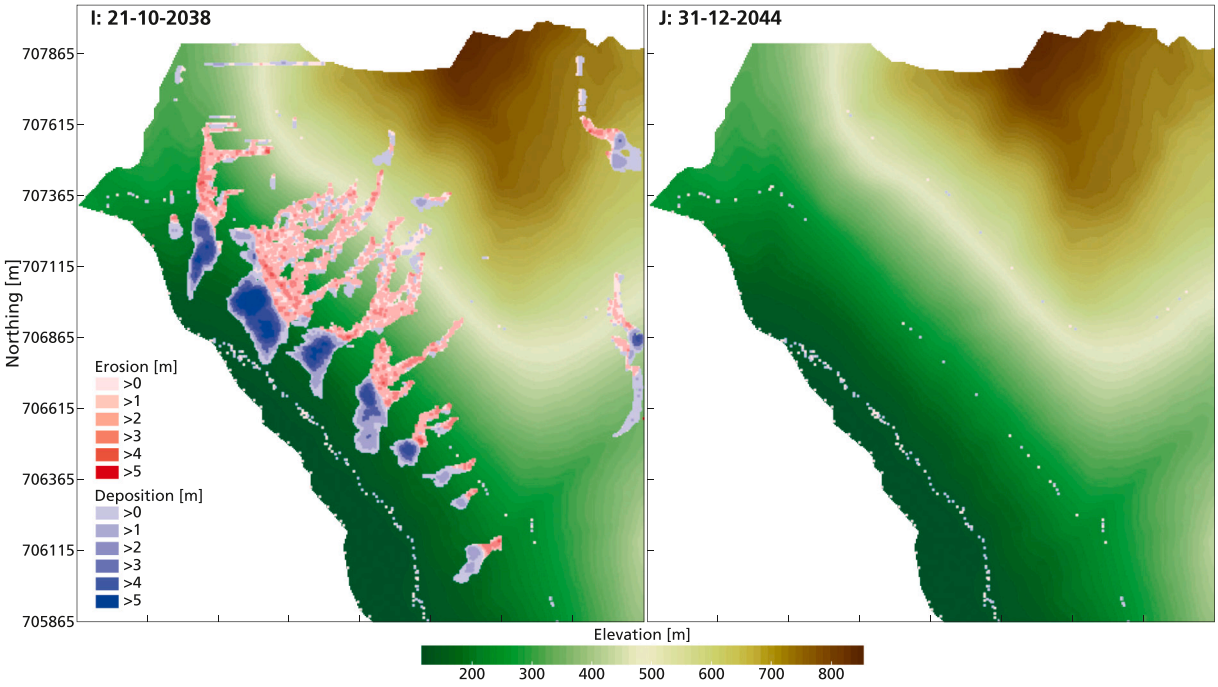

Fig. D.1. (*continued*).

References

Allen, R.G., Pereira, L.S., Raes, D., Smith, M., et al., 1998. Crop evapotranspiration-guidelines for computing crop water requirements-FAO irrigation and drainage paper 56. Fao, Rome 300 (9), D05109.

Andrew, A.M., 1979. Another efficient algorithm for convex hulls in two dimensions. Inf. Process. Lett. 9 (5), 216–219.

Bainbridge, R., Dunning, S., Lim, M., 2018. Low-cost optical and seismic monitoring of debris-flow hazards on the Rest and Be Thankful, Scotland. In: EGU General Assembly Conference Abstracts, vol. 20, p. 15784.

Balland, V., Pollacco, J.A.P., Arp, P.A., 2008. Modeling soil hydraulic properties for a wide range of soil conditions. Ecol. Model. 219 (3), 300–316.

Ballantyne, C.K., 2002. Paraglacial geomorphology. Quat. Sci. Rev. 21 (18), 1935–2017.

Ballantyne, C.K., 2004. Geomorphological Changes and Trends in Scotland: Debris-flows. Scottish Natural Heritage.

Balzano, B., Tarantino, A., Ridley, A., 2016. Analysis of a rainfall-triggered landslide at Rest and be Thankful in Scotland. E3S Web Conf. 9, 15009.

Barkwith, K.A.P., Coulthard, T.J., 2014. CLiDE V1.0 User Guide. British Geological Survey, Nottingham, United Kingdom.

Barkwith, K.A.P., Hurst, M.D., Jackson, C.R., Wang, L., Ellis, M.A., Coulthard, T.J., 2015. Simulating the influences of groundwater on regional geomorphology using a distributed, dynamic, landscape evolution modelling platform. Environ. Model. Softw. 74, 1–20.

Bates, P.D., Horritt, M.S., Fewtrell, T.J., 2010. A simple inertial formulation of the shallow water equations for efficient two-dimensional flood inundation modelling. J. Hydrol. 387 (1), 33–45.

Bee, E.J., Dashwood, C., Pennington, C., Ciurean, R.L., Lee, K., 2019. Creating a national scale debris flow susceptibility model for Great Britain: a GIS-based heuristic approach. Nat. Hazards Earth Syst. Sci. Discuss. https://doi.org/10.5194/nhess-2019-54 (preprint).

BGS Landslide Team, 2018. National landslide database. https://www.bgs.ac.uk/landslides/nld.html. (Accessed 20 October 2023).

Boorman, D., Hollis, J., Lilly, A., 1995. Hydrology of Soil Types: A Hydrologically-based Classification of the Soils of United Kingdom. Institute of Hydrology.

Bown, C.J., Shipley, B.M., Bibby, J.S., 1982. South-West Scotland: soil and land capability for agriculture. Soil Surv. Scotl. 6, 14–122.

Brayshaw, D., Hassan, M.A., 2009. Debris flow initiation and sediment recharge in gullies. Geomorphology 109 (3), 122–131.

Bruce, J.P., Clark, R.H., 1966. Introduction to hydrometeorology. In: Pergamon International Library of Science, Technology, Engineering and Social Studies. Elsevier Science.

Chan, S.C., Kahana, R., Kendon, E.J., et al., 2018. Projected changes in extreme precipitation over Scotland and Northern England using a high-resolution regional climate model. Clim. Dyn. 51, 3559–3577. https://doi.org/10.1007/s00382-018-4096-4.

Chen, C.-W., Oguchi, T., Chen, H., Lin, G.-W., 2018. Estimation of the antecedent rainfall period for mass movements in Taiwan. Environ. Earth Sci. 77 (5), 184.

Chertkov, V.Y., 2002. Modelling cracking stages of saturated soils as they dry and shrink. Eur. J. Soil Sci. 53 (1), 105–118.

Christierson, B.V., Vidal, J., Wade, S.D., 2012. Using UKCP09 probabilistic climate information for UK water resource planning. J. Hydrol. 424-425, 48–67.

Cosma, S., Richard, E., Miniscloux, F., 2006. The role of small-scale orographic features in the spatial distribution of precipitation. Q. J. R. Meteorol. Soc. 128 (579), 75–92.

Coulthard, T.J., Van de Wiel, M.J., 2006. A cellular model of river meandering. Earth Surf. Process. Landf. 31 (1), 123–132.

Coulthard, T.J., Neal, J.C., Bates, P.D., Ramirez, J., Almeida, G.A.M., Hancock, G.R., 2013. Integrating the LISFLOOD-FP 2D hydrodynamic model with the CAESAR model: implications for modelling landscape evolution. Earth Surf. Process. Landf. 38 (15), 1897–1906.

Crosta, G.B., Frattini, P., 2001. Rainfall thresholds for triggering soil slips and debris flow. In: Proc. of the 2nd EGS Plinius Conference on Mediterranean Storms: Publication CNR GNDCI, vol. 2547, pp. 463–487.

Dahal, R.K., Hasegawa, S., 2008. Representative rainfall thresholds for landslides in the Nepal Himalaya. Geomorphology 100 (3), 429–443.

D'Ambrosio, D., Di Gregorio, S., Iovine, G., 2003. Simulating debris flows through a hexagonal cellular automata model: SCIDDICA S_{3-hex}. Nat. Hazards Earth Syst. Sci. 3 (6), 545–559.

Estabragh, A., Moghadas, M., Moradi, M., Javadi, A., 2017. Consolidation behavior of an unsaturated silty soil during drying and wetting. Soils Found. 57 (2), 277–287.

Faurès, J.-M., Goodrich, D.C., Woolhiser, D.A., Sorooshian, S., 1995. Impact of small-scale spatial rainfall variability on runoff modeling. J. Hydrol. 173 (1), 309–326.

Finlayson, A., 2020. Glacial conditioning and paraglacial sediment reworking in Glen Croe (the Rest and be Thankful), western Scotland. Proc. Geol. Assoc. 131 (2), 138–154.

Foley, A., 2010. Uncertainty in regional climate modelling: a review. Prog. Phys. Geogr. 34 (5), 647–670.

Glade, T., Crozier, M.J., Smith, P., 2000. Applying probability determination to refine landslide-triggering rainfall thresholds using an empirical "antecedent daily rainfall model". Pure Appl. Geophys. 157 (6), 1059–1079.

Hadley Centre for Climate Prediction and Research, 2008. UKCP 09: Met Office Hadley Centre Regional Climate Model HadRM3-PPE Data. NCAS British Atmospheric Data Centre.

Harding, A., Rivington, M., Mineter, M., Tett, S., 2015. Agro-meteorological indices and climate model uncertainty over the UK. Clim. Chang. 128 (1–2), 113–126.

Hearn, G.J., 2011. Slope engineering for mountain roads. In: GSL Engineering Geology Special Publications. Geological Society of London.

Hearn, G.J., Massey, C.I., 2009. Engineering geology in the management of roadside slope failures: contributions to best practice from Bhutan and Ethiopia. Q. J. Eng. Geol. Hydrogeol. 42 (4), 511–528.

Heath, R.C., 1983. Basic Ground-water Hydrology: US Geological Survey Water-supply Paper 2220. US Geological Survey, Washington, DC.

Heimsath, A.M., Dietrich, W.E., Nishiizumi, K., Finkel, R.C., 1997. The soil production function and landscape equilibrium. Nature 388 (6640), 358.

Heimsath, A.M., Dietrich, W.E., Nishiizumi, K., Finkel, R.C., 2001. Stochastic processes of soil production and transport: erosion rates, topographic variation and cosmogenic nuclides in the Oregon Coast Range. Earth Surf. Process. Landf. 26 (5), 531–552.

Holmes, C., Tett, S., Butler, A., 2017. What is the uncertainty in degree-day projections due to different calibration methodologies? J. Clim. 30 (22), 9059–9075.
Intermap Technologies, 2007. NEXTMap British Digital Terrain Model Dataset produced by Intermap, NERC Earth Observation Data Centre. http://catalogue.ceda.ac.uk/uuid/8f6e1598372c058f07b0aeac2442366d.
Iverson, R.M., 2000. Landslide triggering by rain infiltration. Water Resour. Res. 36, 1897–1910.
Jaiswal, P., van Westen, C.J., 2009. Estimating temporal probability for landslide initiation along transportation routes based on rainfall thresholds. Geomorphology 112 (1–2), 96–105.
Kay, A.L., Jones, R.G., 2012. Comparison of the use of alternative UKCP09 products for modelling the impacts of climate change on flood frequency. Clim. Chang. 114 (2), 211–230.
Kean, J.W., McCoy, S.W., Tucker, G.E., Staley, D.M., Coe, J.A., 2013. Runoff-generated debris flows: observations and modeling of surge initiation, magnitude, and frequency. J. Geophys. Res. Earth 118 (4), 2190–2207.
Kirkby, M.J., 1967. Measurement and theory of soil creep. J. Geol. 75 (4), 359–378.
Kirschbaum, D., Adler, R., Adler, D., Peters-Lidard, C., Huffman, G., 2012. Global distribution of extreme precipitation and high-impact landslides in 2010 relative to previous years. J. Hydrometeorol. 13 (5), 1536–1551.
Kjekstad, O., Highland, L., 2009. Economic and social impacts of landslides. In: Landslides–Disaster Risk Reduction. Springer, pp. 573–587.
Klaassen, B., Pilgrim, D.H., 1975. Hydrograph recession constants for New South Wales streams. Civ. Eng. Trans. 43–49.
Kromer, R.A., Hutchinson, D.J., Lato, M.J., Gauthier, D., Edwards, T., 2015. Identifying rock slope failure precursors using lidar for transportation corridor hazard management. Eng. Geol. 195, 93–103.
Macklin, C., 2013. A83 Trunk Road Route Study. Jacobs UK Ltd.
Martin, Y., 2000. Modelling hillslope evolution: linear and nonlinear transport relations. Geomorphology 34 (1–2), 1–21.
Marui, H., International Research Society Interpraevent, 2006. Disaster mitigation of debris flows, slope failures and landslides. In: Proceedings of the INTERPRAEVENT International Symposium Disaster Mitigation of Debris Flows, Slope Failures and Landslides Held on September 25-27, 2006, in Niigata, Japan. Frontiers Science Series. Universal Acad. Press, p. 2.
McMillan, F.N., Holt, C.A., 2019. BEAR Scotland NW trunk road maintenance: efficient management of geotechnical emergencies. Q. J. Eng. Geol. Hydrogeol. 52 (3), 286–294.
McQuaker, G., Graeme Herd, J., Johnston, K., 2014. Can We Rest and Be Thankful Yet? Solutions and Effective Stakeholder Engagement for the A83 Trunk Road Route Study. Technical Report. Scotland Transport.
MetOffice, 2019. UK climate averages. https://www.metoffice.gov.uk/research/climate/maps-and-data/uk-climate-averages. (Accessed 9 October 2023).
Monsieurs, E., Dewitte, O., Depicker, A., Demoulin, A., 2019. Towards a transferable antecedent rainfall—susceptibility threshold approach for landsliding. Water 11 (11), 2202. https://doi.org/10.3390/w11112202.
Morgan, R., Quinton, J., Smith, R., Govers, G., Poesen, J., Auerswald, K., Chisci, G., Torri, D., Styczen, M., 1998. The european soil erosion model (eurosem): a dynamic approach for predicting sediment transport from fields and small catchments. Earth Surf. Process. Landf. J. Br. Geomorphol. Group 23 (6), 527–544.
Morris, D.A., Johnson, A.I., 1967. Summary of Hydrologic and Physical Properties of Rock and Soil Materials, as Analyzed by the Hydrologic Laboratory of the US Geological Survey, 1948-60. Technical Report. US Govt. Print. Off.
Murphy, J.M., Booth, B.B.B., Collins, M., Harris, G.R., Sexton, D.M.H., Webb, M.J., 2007. A methodology for probabilistic predictions of regional climate change from perturbed physics ensembles. Philos. Trans. R. Soc. Lond. A Math. Phys. Eng. Sci. 365 (1857), 1993–2028.
Murphy, J., Sexton, D., Jenkins, G., Booth, B., Brown, C., Clark, R., Collins, M., Harris, G., Kendon, E., Betts, R., Brown, S., Humphrey, K., McCarthy, M., McDonald, R., Stephens, A., Wallace, C., Warren, R., Wilby, R., Wood, R., 2009. UK Climate Projections Science Report: Climate Change Projections. Meteorological Office Hadley Centre, Exeter, UK.
Ng, C.W., Wang, B., Tung, Y.-K., 2001. Three-dimensional numerical investigations of groundwater responses in an unsaturated slope subjected to various rainfall patterns. Can. Geotech. J. 38 (5), 1049–1062.
Otto, F.E., van der Wiel, K., van Oldenborgh, G.J., Philip, S., Kew, S.F., Uhe, P., Cullen, H., 2018. Climate change increases the probability of heavy rains in Northern England/Southern Scotland like those of storm desmond—a real-time event attribution revisited. Environ. Res. Lett. 13 (2), 024006.
Parker, R.N., Hales, T.C., Mudd, S.M., Grieve, S.W.D., Constantine, J.A., 2016. Colluvium supply in humid regions limits the frequency of storm-triggered landslides. Sci. Rep. 6, 34438. https://doi.org/10.1038/srep34438.
Pelletier, J.D., Rasmussen, C., 2009a. Geomorphically based predictive mapping of soil thickness in upland watersheds. Water Resour. Res. 45 (9).
Pelletier, J.D., Rasmussen, C., 2009b. Quantifying the climatic and tectonic controls on hillslope steepness and erosion rate. Lithosphere 1 (2), 73–80.
Pennington, C., Dijkstra, T.A., Lark, M., Dashwood, C., Harrison, A., Freeborough, K., 2014. Antecedent precipitation as a potential proxy for landslide incidence in South West United Kingdom. In: Sassa, K., Canuti, P., Yin, Y. (Eds.), Landslide Science for a Safer Geoenvironment. Cham. Springer International Publishing, pp. 253–259.
Postance, B., Hillier, J., Dijkstra, T.A., Dixon, N., 2017. Extending natural hazard impacts: an assessment of landslide disruptions on a national road transportation network. Environ. Res. Lett. 12 (1), 014010.
Prellwitz, R.W., 1981. Transportation engineering handbook, Region 1. In: Number 11 in Transportation Engineering Handbook. U.S. Department of Agriculture, Forest Service, Northern Region.
Prellwitz, R.W., Koler, T.E., Steward, J.E., Hall, D.E., Long, M.T., Remboldt, M.D., United States. Forest Service. Engineering Staff, 1994. Slope stability reference guide for national forests in the United States. In: Number v. 2 in Slope Stability Reference Guide for National Forests in the United States. U.S. Department of Agriculture, Forest Service, Engineering Staff.
Rayner, B., Nicoll, B., 2012. Potential for woodland restoration above the A83 in Glen Croe to reduce the incidence of water erosion and debris flows. For. Res. 1–24.
Sanderson, M.G., 2010. Changes in the Frequency of Extreme Rainfall Events for Selected Towns and Cities. Ofwat, UK.
Sanderson, M.G., Wiltshire, A.J., Betts, R.A., 2012. Projected changes in water availability in the United Kingdom. Water Resour. Res. 48 (8).
Schlögl, M., Matulla, C., 2018. Potential future exposure of european land transport infrastructure to rainfall-induced landslides throughout the 21st century. Nat. Hazards Earth Syst. Sci. 18 (4), 1121–1132.
Scottish Environmental Protection Agency, 2017. Private Communication. Scottish Environmental Protection Agency.
Selby, M.J., 1982. Hillslope Materials and Processes. Oxford University Press.
Smakhtin, Y.V., Masse, B., 2000. Continuous daily hydrograph simulation using duration curves of a precipitation index. Hydrol. Process. 14 (6), 1083–1100.
Sparkes, B., Dunning, S., Lim, M., Winter, M.G., 2017. Characterisation of recent debris flow activity at the Rest and Be Thankful, Scotland. In: Advancing Culture of Living With Landslides. Springer International Publishing, Cham, pp. 51–58.
Sun, W.-J., Cui, Y.-J., 2018. Investigating the microstructure changes for silty soil during drying. Geotechnique 68 (4), 370–373.
Tanner, P.G., Thomas, C.W., Harris, A.L., Gould, D., Harte, B., Treagus, J.E., Stephenson, D., 2013. The Dalradian rocks of the Highland Border region of Scotland. Proc. Geol. Assoc. 124 (1), 215–262.
The Dalradian Rocks of Scotland. Transport Scotland, 2018. Scottish trunk road network asset management strategy. https://www.transport.gov.scot/transport-network/roads/the-trunk-road-network/. (Accessed 2 July 2019).
Transport Scotland, 2021. The Trunk Road Network. https://www.transport.gov.scot/transport-network/roads/the-trunk-road-network/. (Accessed 2 July 2019).
Tsai, T.-L., 2008. The influence of rainstorm pattern on shallow landslide. Environ. Geol. 53 (7), 1563–1569.
Van Asch, T.W.J., Buma, J., Van Beek, L.P.H., 1999. A view on some hydrological triggering systems in landslides. Geomorphology 30 (1–2), 25–32.
Van Asch, T.W.J., Van Beek, L.P.H., Bogaard, T.A., 2009. The diversity in hydrological triggering systems of landslides. In: Proceedings of The First Italian Workshop on Landslides, pp. 8–10.
Winter, M.G., 2014. A strategic approach to landslide risk reduction. Int. J. Landslide Environ. 2 (1), 14–23.
Winter, M.G., 2020. Debris flows. Geol. Soc. Lond. Eng. Geol. Spec. Publ. 29 (1), 163–185.
Winter, M.G., Corby, A., 2012. A83 Rest and be Thankful: ecological and related landslide mitigation options. A83 Rest and be Thankful: Ecological and Related Landslide Mitigation Options 1 (1), 1–26.
Winter, M.G., Shearer, B., 2017. An extended and updated technical evaluation of wig-wag signs at the A83 rest and be thankful. Published project report. In: PPR, 743. Transport Research Laboratory, Wokingham, ISBN 978-1-910377-74-1, p. 36.
Winter, M.G., Macgregor, F., Shackman, L. (Eds.), 2008. Scottish Road Network Landslides Study: Implementation. Transport Scotland, Edinburgh, p. 278, 978-906106-38-9.
Winter, M.G., Dent, J., Macgregor, F., Dempsey, P., Motion, A., Shackman, L., 2010. Debris flow, rainfall and climate change in Scotland. Q. J. Eng. Geol. Hydrogeol. 43, 429–446.
Winter, M.G., Shearer, B., Palmer, D., Peeling, D., Harmer, C., Sharpe, J., 2016. The economic impact of landslides and floods on the road network. Procedia Eng. 143, 1425–1434.
Winter, M.G., Shearer, B., Palmer, D., Peeling, D., Peeling, J., Harmer, C., Sarpe, J., 2018. Assessment of the economic impacts of landslides and other climate-driven events. In: TRL Published Project Report PPR878.
Wong, J.C.F., Winter, M.G., 2018. The Quantitative Assessment of Debris Flow Risk to Road Users on the Scottish Trunk Road Network: A83 Rest and be Thankful (No. PPR798).